To the Graduate Council:

I am submitting herewith a dissertation written by Charles Frederick Weber entitled "A Solubility Model for Aqueous Solutions Containing Sodium, Fluoride, and Phosphate." I have examined the final copy of this dissertation for form and content and recommend that it be accepted in partial fulfillment of the requirements for the degree of Doctor of Philosophy, with a major in Chemical Engineering.

J. S. Watson

J. S. Watson, Major Professor

We have read this dissertation
and recommend its acceptance:

Robert M. Counce

Joseph J. Perona

M. H. Lietzke

Accepted for the Council:

Lew Winkel

Associate Vice Chancellor and
Dean of The Graduate School

A SOLUBILITY MODEL FOR AQUEOUS SOLUTIONS CONTAINING SODIUM, FLUORIDE, AND PHOSPHATE

A Dissertation
Presented for the
Doctor of Philosophy
Degree
The University of Tennessee, Knoxville

Charles Frederick Weber

May 1998

DEDICATION

This dissertation is dedicated to my wife,

Renee R. Weber,

for her patience and encouragement

in the completion of this degree

and in the whole of life.

ACKNOWLEDGMENTS

The author is greatly indebted to several staff members of the Oak Ridge National Laboratory for assistance in this effort. Especially significant was the encouragement of longtime friend and colleague Ed Beahm. As project leader, he provided general direction and arrangements for this work as a part of overall program goals. Mike Simonson provided valuable advice on modeling the dilution enthalpy of reacting systems. Doug Lee and Tom Dillow were primarily responsible for performing the experimental work in Section 5. Lindy Norris and Willena Carter spent considerable time and effort typing the many drafts of this thesis.

Appreciation is also directed to J. S. Watson for many helpful suggestions and to committee members J. J. Perona, M. H. Lietzke, and R. M. Counce for their service. Finally, the author is greatly indebted to Lockheed Martin Energy Research Corporation and the U.S. Department of Energy for their support of higher education generally, and for the specific assistance received in accomplishing this work.

ABSTRACT

A computational model is developed to calculate thermodynamic phase equilibria in aqueous solutions of fluoride, phosphate, and hydroxide up to 100°C. A variety of data are used, including isopiestic and e.m.f. measurements, freezing point data, vapor pressure data at 100°C, heat capacities, heats of dilution, and solubility measurements. Pitzer's ion-interaction treatment is used to model electrolyte solutions, and many unknown parameters are determined from existing data through nonlinear least squares fitting. Phase equilibria are determined by minimization of total free energy using a modification of the code SOLGASMIX. Results calculated using the model accurately predict phase equilibria from many quantitative experiments. Qualitative experiments are performed to evaluate calculated solubilities in regions of sparse or nonexistent data; the calculated results are reasonable and exhibit general qualitative agreement with such data. Model predictions are useful in understanding problems that may arise in the treatment of waste streams containing fluoride and phosphate anions in highly caustic solutions.

TABLE OF CONTENTS

LIST OF FIGURES

FIGURE PAGE

LIST OF TABLES

SECTION 1

INTRODUCTION

During the past 50 years, a considerable accumulation of liquid radioactive and hazardous wastes has occurred at various research facilities operated by subcontractors of the U.S. Government. Some of the wastes resulted from defense-related work, although other research activities also contributed. Progressive declassification of government operations over the last two decades has increased public awareness and concern about the health and environmental threats posed by continued storage of these wastes. In addition, recent world political events have allowed the redirection of funding and attention to address the many scientific and technological issues.

Generally, waste streams from a variety of processes were collected together in common holding tanks, and little record exists of the original substances. Chemical reactions between different wastes or between wastes and structures (pipes, tanks, etc.) were not considered. In some cases, sufficient corrosion has occurred that tanks have leaked radioactive and hazardous material to the environment. Most of the waste tank inventories are highly concentrated, due to some processing that has occurred. Because little is known about the wastes that entered a given tank, a thorough characterization of each tank is necessary, including radioactive nuclides present and dominant chemical species.

Samples of several tanks have yielded a good qualitative understanding of the contents. Most tanks have high pH (12-14) due to addition of NaOH to control corrosion, and also contain high inventories of various ions (Na^+ and NO_3^- are especially predominant). At various times, certain species precipitated and settled out, creating layers of sludge at the bottom of the tanks. In some cases, several different sludge layers exist, and it is possible that none is in true thermodynamic equilibrium with the overlying liquid currently in the tank. The consistencies and compositions of the sludge layers vary from tank to tank, although there are some common features. In addition, trace quantities of radioactive nuclides are present which pose significant problems for ultimate processing and disposal. Wastes at the Hanford National Engineering Laboratory (HNEL) are of prime concern, and often contain large quantities of aluminum and $BiPO_4$, together with various anions, including F^-.

A significant problem in the processing of these wastes is uncontrolled precipitation in solutions containing hydroxide, fluoride, and phosphate ions. For example, the treatment of radioactive sludge from Hanford underground storage tanks will likely involve leaching with additional sodium hydroxide solution. Failure to understand and control precipitation could result in the formation of crystalline solids and gels that are unacceptable because they will prevent mixing, impede pumping, retard separations, coat surfaces, and clog pipes, equipment, and filters. This issue is of great practical concern, since solids containing both phosphate and fluoride have been found in several caustic leaching tests on sludge from the Hanford tanks.

It is generally understood that the presence of even small amounts of fluoride or phosphate will drastically affect the solubility of the other anion. However,

quantification of mutual solubility effects has been hampered by the paucity of data, conflicting data, and failure to account for phosphate hydrolysis and excess hydroxide. The present effort is driven by the need to characterize aqueous mixed waste containing Na^+, F^-, PO_4^{-3}, HPO_4^{-2}, and OH^-, and to evaluate various processing strategies. This requires modeling such systems to 100°C and at high caustic concentrations.

Such a comprehensive modeling effort has not previously been undertaken. However, numerous researchers have studied a subset of the problem, and a variety of data exist. Such work is noted in Section 2, where the usefulness of various types of data is also discussed. Mathematical modeling and numerical calculation are discussed in Section 3, as they apply to electrolyte thermodynamics, chemical equilibrium, and parameter estimation. Specific model parameters are determined in Section 4 by applying nonlinear least-squares estimation to fit data of various subsystems. Finally, the model is used to estimate sodium-fluoride-phosphate solubilities in Section 5; it is also compared to qualitative data that reflect realistic sludge processing conditions.

SECTION 2

BACKGROUND

The purpose of this study is to develop a comprehensive description of the aqueous electrolyte system:

$$Na - F - PO_4 - HPO_4 - OH - H_2O \qquad (1)$$

in the temperature range 25-100°C. Since measurements are both difficult and expensive, it is important to utilize existing data as much as possible; hence, any data involving one or more of the above constituents will be considered. Ultimately, it is also necessary to evaluate the usefulness and consistency of all data. This will be done in Section 4, as part of the parameter estimation process. Here, previous work is mentioned that has addressed some subset or related area to our problem of concern. A data variance is assigned to each point or group of points, in anticipation of use in the quantitative analysis described in Sections 3 and 4.

2.1 Common Electrolyte Systems

An exhaustive evaluation of the binary system Na-OH has been performed by Simonson et al.[1] These authors utilized a variety of activity data, enthalpy data, and heat capacities to construct a rigorous and comprehensive model over the temperature range

0-525°C and at pressures up to 20 kpa. Their results are used here, applied to more limited conditions (atmospheric pressure, 0-100°C).

Numerous studies of Na-Cl aqueous systems have been performed. While the present study does not involve Cl^- directly, some additional mixed salt data are available if this anion is included. Since it has been characterized thoroughly, it poses little additional effort to do so. Hence, the model results given in Pitzer[2] are used, again applied within the temperature and pressure limits of this study.

2.2 Subsystems Involving Na-F

Considerable data are available for the Na-F system, and are listed in Table 1. However, there are many discrepancies, even among measurements which are usually regarded as quite accurate. For example, Fig. 1 shows solubilities in the binary solution in the temperature range 0-100°C. The dashed line represents a fit by Linke[3] of many early results, and he notes that there was considerable scatter in the data used. The more recent data shown in Fig. 1 also show considerable scatter and seem to indicate systematic, rather than random, error. In particular, the results of Guiot[4] seem artificially low, which is disappointing. This author also has a large quantity of data for the $Na\text{-}PO_4\text{-}F$ system, which is somewhat questionable in view of these NaF results.

Activity coefficients at 25°C have been measured by both isopiestic[5] and e.m.f.[6] experiments. Although both techniques are quite effective, these two data sets are somewhat inconsistent with each other. Hamer and Wu[7] seem to favor the former, and their smoothed values more closely match these results. In this study, there is no compelling reason to choose one over the other *a priori*. Since a great variety of other

Table 1. Data used to characterize NaF aqueous systems

Ref.	Data type	Range of validity		Fitted para-meter	Data vari-ance	Number of Points
		I (m)	T (°C)			
Binary system						
5	isopiestic	0.1-1.0	25	φ	10^{-5}	6
6	e.m.f.	0.05-0.9	15-35	γ	3×10^{-5}	15
8	freezing pt. depression	0.04-0.5	0	φ	5×10^{-4}	5
9	vapor pressure	0.24-1.07	100	φ	10^{-5}	5
11	enthalpy of dilution	0.004-1.07	25	ΔH_{dil}	0.1	26
11	heat capacity	0.08-0.72	25	C_p	0.01	11
3	binary solubilities	~1	0-100°C	m_i	10^{-3}	6
Data in mixed systems						
12	Na-Cl-F solubility	1-6.2	25, 35	m_i	10^{-3}	7
13	Na-Cl-F solubility	1-6.2	50	m_i	10^{-3}	10
15	Na-OH-F solubility	1-1.4	0,40,80,94	m_i	10^{-3}	16
15	Na-OH-F solubility	1-5.7	20	m_i	10^{-3}	8
16	Na-Cl-F e.m.f.	1-6	25	γ	3×10^{-5}	25

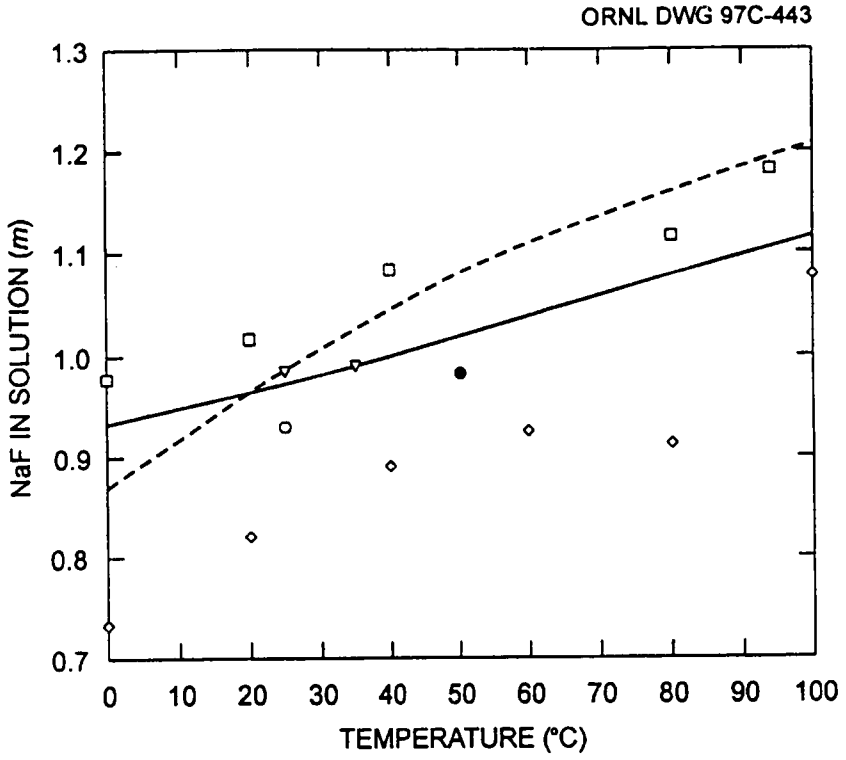

Figure 1. NaF Binary System Solubilities. □ Ref. 15, ○ Ref. 14, ● Ref. 13, ◇ Ref. 4, ▽ Ref. 12, --- Ref. 3, — this study.

data is involved, the two sets are weighted nearly the same. Whichever is favored depends on consistency with the other data involved.

Additional binary system data are used to evaluate activity coefficients at other temperatures. Direct activity measurements arise from freezing point lowering[8], vapor pressure measurements[9] at 100°C, and the e.m.f. data[6] at 15 and 35°C. Freezing point data are translated into values of osmotic coefficient using the correlation of Robinson and Stokes[10]

$$\varphi = \frac{\Delta T}{m}\,(0.5377 + 0.0002684\,\Delta T)\,, \qquad (2)$$

where ΔT = the temperature lowering of the freezing point (K), and m = total ions in solution (assuming complete dissociation). Measurements of dilution enthalpy and heat capacities[11] help establish the temperature dependence, even though they occur only at 25 °C.

In addition to the binary data, several researchers have considered systems involving Na^+, F^- and a third ion. Such systems are particularly useful, since they involve ionic strengths well above the NaF solubility limit, and also allow estimation of ternary mixture parameters and free energies of formation. Solubility data are available for Na-Cl-F systems,[12–14] and Na-OH-F systems.[15] Because there appear to be serious inconsistencies in the data of Campbell,[14] they were not actually included in this analysis, and do not appear in Table 1. The data in hydroxide solutions are especially useful, since they span the temperature range 0-100 °C, although they extend above I = 1.5 only at 20 °C. In addition, mixture e.m.f. data[16] are available for Na-Cl-F systems at 25 °C; while they do not help determine temperature coefficients or free energies, these data contribute to determination of both binary parameters at high ionic strengths and ternary mixture parameters.

2.3 The Binary System Na-HPO_4

Because very little hydrolysis occurs, this system can be regarded as a binary system. It is, of course, a prerequisite to evaluating the systems involving PO_4^{-3}.

Available data for Na_2HPO_4, are shown in Table 2. The isopiestic results of Platford,[17] and Scatchard and Breckinridge,[18] at 25 °C are in quite good agreement

Table 2. Data used for Na_2HPO_4

Ref.	Data type	Range of validity		Fitted para-meter	Data vari-ance	Number of points
		I (m)	T (°C)			
22	Freezing point depression	0.035-0.11	0	φ	10^{-4}	3
23	Freezing point depression	0.01-0.1	0	φ	10^{-4}	4
24	Vapor pressure data	0.53-3.8	100	φ	5×10^{-5}	8
25	Vapor pressure data	0.5-4.0	100	φ	5×10^{-5}	5
18	Isopiestic	0.09-1.0	25	φ	10^{-6}	25
17	Isopiestic	0.23-2.1	25	φ	10^{-6}	10
19	Dilution enthalpy	0.06-0.5	30	ΔH_{dil}	0.3-1.0	12
20, 21	Heat capacity	0.06-0.7	25	C_p	0.1	10

with each other, and have been assigned a small variance, consistent with this agreement and with the authors' estimates of experimental error. The dilution enthalpy measurements of Millero et al.,[19] also appear to be quite consistent with other data, and have been assigned variable variances from 0.3 for higher concentrations to 1 for the lowest concentrations, consistent with the author's recognition of uncertainty in their data. Bianchi and Tremaine[20] and Larson[21] used flow calorimetry to measure apparent molar heat capacities for mixed solutions containing both Na_2HPO_4 and NaH_2PO_4, with Na_2HPO_4 mole fraction of total solute: $x = 0.15$, 0.5, and 0.9. Extrapolation to $x = 1$ yielded approximate values for apparent molar heat capacities for pure Na_2HPO_4 solutions. Osmotic coefficients at the freezing point were determined from Eq. (2), applied to the freezing point data in Refs. 22 and 23. The origin of the CRC data is not given, and it is possible that Ref. 23 is the primary source. In any event, the two are quite

consistent with each other and both were used. The fairly large variance reflects the uncertainty in origin and experimental methods.

Vapor pressure lowering at 100°C yields osmotic coefficients for a large range of concentrations. As in the case of freezing points, there may be a nebulous connection between the data of Refs. 24 and 25, which agree closely with each other. The table of values in Ref. 25 also appears in Ref. 22, and neither makes reference to the original source of the data. Ref. 25 is alleged to be an updated version of the *International Critical Tables*,[9] published in 1928. Here, there is explicit reference to Ref. 24, implying that Refs. 24 and 25 actually represent the same data. As with freezing point data, both sets of values are used, and a variance chosen to reflect uncertainty in origin and accuracy of the early measurements.

2.4 The System $Na\text{-}PO_4\text{-}HPO_4\text{-}OH$

Solid trisodium phosphate (TSP) is known to contain water of hydration and possibly excess caustic. The dodecahydrate is commonly recognized:

$$Na_3PO_4 \cdot 12H_2O. \tag{3a}$$

Wendrow and Kobe[26] conducted an extensive review and concluded that the formula is actually

$$Na_3PO_4 \cdot 12H_2O \cdot \tfrac{1}{4}NaOH, \tag{3b}$$

if crystallization has occurred below about 70°C and with a Na/PO_4 ratio of about 3 or higher. Such is usually the case, and even reagent grade TSP recognizes the presence of

up to 2.5% excess caustic. Since the exact amount is not usually quantified, experiments using reagent TSP may produce erratic results. To avoid this difficulty, some researchers avoid reagent TSP, and mix NaOH with H_3PO_4 or Na_2HPO_4 in stoichiometric amounts. This creates a system which is known more exactly.

In general, it is necessary to consider the hydrolysis of phosphate according to the reaction:

$$PO_4^{-3} + H_2O \leftrightarrow HPO_4^{-2} + OH^-. \qquad (4)$$

It is thus impossible to consider solutions of TSP as simple binary systems, since they will necessarily contain OH^-, or HPO_4^{-2}, or both. The binary systems NaOH and Na_2HPO_4 have already been discussed, and will be used in the complete evaluation of thermodynamic parameters for Na_3PO_4 in aqueous solutions.

A variety of data are available for TSP solutions, although the quality varies, and very little exists at temperatures different from 25°C. Data considered for this study are listed in Table 3, where it is noted that only References 18–20, and 26 completely specify the solution composition.

The isopiestic data[18] are highly reliable, involving well defined buffer systems in which the hydrolysis reaction (4) can be neglected. As was the case with Na-HPO_4 systems, the only activity data at temperatures other than 25°C are measurements of freezing point depression and vapor pressures at 100°C. All such data are quite old and consist of only a few points. Loomis[23] describes the process whereby solid TSP was crystallized in excess NaOH, probably implying the form (3b). He mentions the inability to reconcile his results with the pure dodecahydrate (3a). Again it is likely that data from

Table 3. Data for Na_3PO_4 aqueous solutions

Ref.	Data type	Range of validity		No. of points	Solution composition
		T (°C)	I (m)		
18	Isopiestic	25	0.4–4.0	20	$Na_3PO_4 + Na_2HPO_4$
23	Freezing point	0	0.06–0.6	4	Na_3PO_4 + excess NaOH
22	Freezing point	0	0.2–1.0	5	Unknown
24	Vapor pressure	100	2.3–12.6	5	Unknown
25	Vapor pressure	100	3.0–12.0	3	Unknown
19	Dilution enthalpy	30	0.08–3.0	20	Stoich. mixture: $NaOH + H_3PO_4$
20	Heat capacity	25	0.3–2.8	6	Stoich. mixture: $NaOH + H_3PO_4$
21	Heat capacity	25	0.1–1.0	7	Reagent TSP
26	Solubility	0–60	2.0–9.0	33	Mixture: $Na_2O + P_2O_5$

Reference 22 are derived (at least in part) from those in Ref. 23, and are not truly independent. In any event, References 22 and 23 are quite consistent with each other. The form (3b) produced much better modeling results and was assumed for both data sets.

Even less is known about the experimental solutions for vapor pressure data at 100°C. Data from Ref. 24 are more than a century old, and their quality is unknown. Again, Ref. 25 gives no details of experimental conditions and may well be based on Ref. 24. In spite of this uncertainty, there are no other data much above 25°C , and hence, it is useful to include these data insofar as they produce results consistent with the rest. Unlike the freezing point data, assuming the form (3a) produced better results, a

reasonable result for crystallization above 70°C, even though the dodecahydrate is not the favored species at this temperature.

The dependence of activity coefficients on temperature can also be determined using enthalpy and heat capacity data. However, allowance must be made for the thermal effects on the hydrolysis reaction (4). For heat capacity measurements, this has been termed the "relaxation effect" and has been approximated using simplifications and assumptions for the activity coefficients and equilibrium constant.[20, 21] Likewise, similar assumptions were utilized to explain dilution enthalpy data.[19] Since a primary goal of this work is the estimation of activity parameters (and free energies of formation), it is not possible to make such assumptions. Instead, the hydrolysis reaction (4) is incorporated into the overall parameter estimation procedure.

2.5 Fluoride-Phosphate Systems

The thermodynamics of sodium-fluoride-phosphate mixtures is complicated somewhat by the usual presence of hydroxide, making this a truly four component system. Unfortunately, many researchers have not accounted for this additional quantity, which is often present through use of reagent grade TSP. Hence, an important part of this effort has been to estimate hydroxide inventories through heuristic means.

Mason and Ashkroft[27] have reviewed earlier studies dating back to the mid-19th century, in which the double salt $NaF{\cdot}2Na_3PO_4{\cdot}19H_2O$ (hereafter referred to as double salt or DS) was noticed as a dominant crystallization product. Many of the earlier studies were more qualitative, however, Mason and Ashkroft sought to determine invariant points of the solubility curve, and actually performed a quantitative evaluation. Several

more recent sources of data are also available, and are listed in Table 4. The first 3 have performed some crystallographic analysis and have concluded that the precipitate is DS, TSP, or NaF. Ref. 29 regards the precipitate as a solid solution of TSP and NaF, based on the changing ratio of F/P. Ref. 30 makes no analysis, but simply assumes the results from Ref. 29. It appears that the weight of evidence favors the formation of DS, and that other factors (such as contamination of samples, unaccounted effects of OH^-, or faulty measurements) have given the appearance of a solid solution. Throughout the remainder of this work, the DS is assumed to be the product formed.

With regard to equilibrium solution concentrations, the various references are not in good agreement, as can be seen from the plot of values at 25°C, shown in Fig. 2. While some of the discrepancies may arise from differences in OH^- concentration (or temperature, in the case of Ref. 4), there are undoubtedly other difficulties as well. In some cases, the measurements were probably taken on systems not in equilibrium. Also, there are certain inconsistencies in some measurements with regard to F/P ratio; most likely these are caused by faulty fluoride measurements. Thus, a major part of this work

Table 4. Data for fluoride-phosphate solubilities

Reference	Temperature (°C)	Usable points
27	25-40	6
28	25-75	17
4	0-100	0
29	25	0
30	100+	5

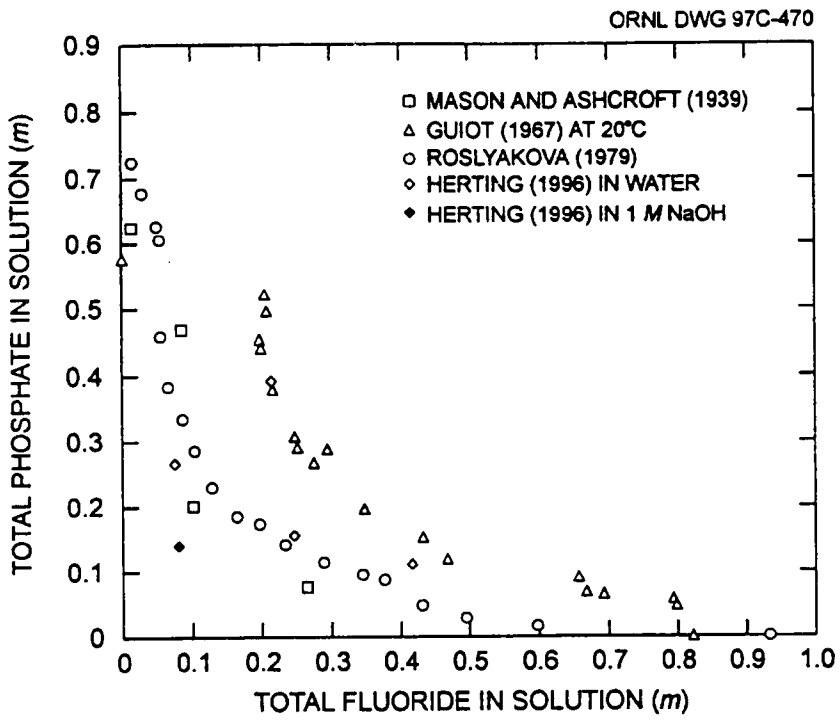

Figure 2. Solubility in the system Na-F-PO_4-OH at 25°C. □ Ref. 27, △ Ref. 4, ○ Ref. 29, ◇ (pure water) and ♦ (in 1 M NaOH) Ref. 28.

is the evaluation of data, and selection of that which can be reliably used in model development.

Most of the researchers do not measure OH^- in their solutions, however, for some it is possible to ascertain reliable values from the descriptions of experimental procedure. For quantitative reliability, this is essential. References 27–30 all mention (or imply) that they use reagent grade TSP without regard to the excess hydroxide. Since this constitutes only 2.5% (by weight) impurity, these researchers reason that the effect is negligible. In order to use such data, the phosphate is assumed to be 20 mol % NaOH, consistent with the research of Wendrow and Kobe,[26] discussed in Section 2.4. In addition, it is necessary to know the exact total inventories of all constituents initially or finally

(including amount of precipitate), since this describes how much OH^- actually is in solution. (Note: Final solution inventories of F^- and PO_4^{-3} are not adequate without knowledge of the amount precipitated, since each mole of PO_4^{-3} precipitated leaves in solution ¼ mol of OH^-, and this quantity is still undefined.) All data from Ref. 27 were used, since the authors state complete initial inventories. Some data from Ref. 28 were also usable — namely those for which quantitative results were obtained. No data from Ref. 29 were used, since it was impossible to adequately determine OH^- concentrations. And finally, the values from Ref. 30 were used, for ionic strengths below 9. This was justified since the experimental procedure describes that sampling is done as soon as the first crystals appear. Hence, the OH^- can be determined from the PO_4^{-3} aqueous inventory, the amount of precipitate being negligible.

In Ref. 4, the author mentions preparation of TSP so as to remove the hydroxide and leave this component in stoichiometric ratio $Na/PO_4 = 3$. This set of data is quite extensive, spanning 0-100°C and involving more than 150 solution measurements, in addition to examination of solid phases and determination of invariant points. Unfortunately, it is not usable, since there are evidently serious errors in many of the values. The pure component solubilities are significantly lower than those of any other researchers, not even lying in the regions of uncertainty for all other available data. Even allowing for uncertainties in OH^- levels, the solubility values in Fig. 2 are quite distant from those of other researchers. Part of the problem may be in the experimental procedure for measuring fluoride. In addition, the author mentions that he determined equilibrium by constancy of solution density, which usually occurred within 12-72 hrs. Mason and Ashkroft[27] mention a solution that initially crystallized to TSP, but that over

the course of one week converted to DS, evidently the more stable form. Likely the solution density remained fairly constant during this time. Thus, it is possible that much of the data from Ref. 4 do not represent a true equilibrium state. This is quite sad, since this author performed an immense amount of labor, and was apparently very thorough in most other respects.

SECTION 3

DESCRIPTION OF CALCULATIONAL MODEL

The vehicle used for building a quantitative model is an adaptation of the chemical equilibrium code SOLGASMIX,[31-34] modified to perform aqueous electrolyte calculations. This code calculates phase equilibrium by minimizing total free energy:

$$G = \sum_i n_i \bar{G}_i = \sum_i n_i \left(G_i^0 + RT \ln a_i \right) \tag{5}$$

where n_i, $\bar{G}_i$, a_i, are the mole inventory, partial molar Gibbs free energy, and activity, respectively, of species i, and the summation includes all components of the system (including water). The molar free energies of formation G_i^0 (equal to the standard chemical potentials μ_i^0) must be obtained from literature or estimated from data. In practice, it is helpful to use the reduced form μ_i^0/RT. The activities are evaluated using the practical system: $a_i = m_i \gamma_i$ (for solutes), and $\ln a = -\varphi \Sigma m_i / \Omega$ where m_i, γ_i, and φ denote molality, activity coefficient, and osmotic coefficient, respectively; for water, $\Omega = 55.51$ moles/kg. If temperature dependent expressions are available for free energies of formation and activity coefficients, then Eq. (5) can be calculated at any temperature.

3.1 Parameter Estimation

A special module has been developed to perform nonlinear optimization, for the purpose of fitting the various parameters to actual data. This procedure uses a combination of Gauss-Newton and the BFGS Quasi-Newton minimization algorithms to minimize squared error as parameter choices vary. For each data set, the phase equilibrium in Eq. (5) is obtained by calling the SOLGASMIX routines.

The optimization is simply a nonlinear least squares procedure[35, 36]

$$\min_{\mathbf{p}} E = \min_{\mathbf{p}} \mathbf{e}^T \mathbf{V} \mathbf{e} \tag{6a}$$

E = total sum of squared error

$\mathbf{p}$ = vector of parameters to be optimized,

$\mathbf{e} = \mathbf{x} - \hat{\mathbf{x}}$ = error vector

$\hat{\mathbf{x}} = (\hat{x}_1, \ldots, \hat{x}_n)^T$ = vector of data points

$\mathbf{x} = (x_1, \ldots, x_n)^T$ = vector of calculated quantities

$\mathbf{V}$ = data covariance matrix.

The elements of the vector $\hat{\mathbf{x}}$ may involve a variety of data: equilibrium solubilities (i.e., aqueous concentrations), osmotic or activity coefficients, enthalpies or heat capacities, etc. Or it may contain quantities derived from such data — logarithms, sums or products, averages, etc. After experimental conditions have been ascertained (i.e., temperature, pressure, total inventories of all components), phase equilibrium is determined. The quantity x_i is then calculated as a prediction of the data $\hat{x}_i$. (Of course, it is possible that more than one data point is related to a single equilibrium calculation.)

If all data points are independent, then the covariance matrix is given by

$$V = \text{diag}\,(\sigma_1^2,\ \sigma_2^2, \ldots,\ \sigma_N^2)$$

where σ_i is the standard deviation of measurement *i*. The total squared error can then be written as

$$E = \sum_{i=1}^{N} (x_i - \hat{x}_i)^2 / \sigma_i^2 \qquad (6b)$$

It is seen in Eq. (6b) that the error contribution of each data point is weighted by the inverse of σ_i^2. This is important both to count "good" data more strongly (i.e., data with a small variance), and to normalize the error contributions of different types of data.

The actual technique used to solve Eq. (6a) is patterned after a procedure in Fletcher.[37] Because of the nonlinearity, iteration is necessary, and the approach uses both the Gauss-Newton and BFGS quasi-Newton methods, together with a step-length calculation.

3.2 Free Energies of Formation

Values for μ_i^0 can be obtained at 25°C from a variety of sources. Because there are disagreements for some species, it is important to recognize that different selection criteria may produce different results. The CODATA[38] selections are favored, since these were obtained through some international consensus, and are particularly applicable to solutions containing uranium and other actinides. While this current study does not involve such elements, the motivation of this work is the ultimate evaluation of mixed waste solutions where actinides may be present. The immediate goal is accurate prediction of phase equilibria, a process which is highly dependent on values of chemical

potential for the species directly involved. Hence, to enhance the model predictions, it may be necessary to make minor adjustments in these and other parameters. Such changes are noted carefully where they deviate from established literature values.

At temperatures different from 25°C, values for free energy of formation can be obtained from various sources; most of these involve some approximation. To begin, values are obtained from the HSC database,[39] since it is well documented and up-to-date. Furthermore, it matches very well the CODATA values for water throughout the temperature range 0-100°C. For present purposes, the HSC data are fit to a nonlinear functional form, as discussed in Sect. 3.3 [cf. Eq. (14)]. Values of the various coefficients used are given in Appendix A.

3.3 Calculation of Activity Coefficients

In order to evaluate activity coefficients, the ion-interaction approach developed by Pitzer[40, 2] is used. Usually termed semi-empirical, Pitzer developed a statistical-mechanical basis for the dependence of the second viral coefficient on ionic strength. He then simplified the approach and developed equations for activity and osmotic coefficients which had adjustable parameters; these are fit empirically to macroscopic data for individual salt solutions or mixtures. The present system contains no neutral species and a single cation Na^+ (actually H^+ is also present, but in such tiny amounts that it need not be considered in the present analysis). It is convenient to index each species as follows:

$$1-H_2O \quad 2-Na^+ \quad 3-PO_4^{3-} \quad 4-HPO_4^{2-} \quad 5-OH^- \quad 6-F^- \,. \tag{7}$$

Then the excess free energy can be expressed by the form[2]

$$\frac{G^{ex}}{M_1 RT} = f(I) + 2 m_2 \sum_{j=3}^{6} m_j \left(B_{2j} + m_2 C_{2j}\right) + \sum_{i=3}^{5} \sum_{j=i+1}^{6} m_i m_j \left(2 \Phi_{ij} + m_2 \psi_{2ij}\right), \quad (8)$$

where M_1 = mass of water (kg)

m_i = molality of species i (mol/kg H_2O)

B_{ij}, C_{ij}, Φ_{ij}, ψ_{ijk} = ion-interaction (Pitzer) parameters.

The quantities Φ_{ij}, and ψ_{ijk} are determined from mixed solutions involving more than one anion. The B_{ij} and C_{ij} are parameters relating a single cation-anion pair, and are most easily determined from a binary salt solution (i.e., a solution not including any other ions). The B_{ij} are determined from the equation

$$B_{ij} = \beta_{ij}^{(0)} + \beta_{ij}^{(1)} g\left(\alpha \sqrt{I}\right), \qquad g(x) = \frac{2}{x^2}\left[1 - (1 + x)e^{-x}\right]. \quad (9a)$$

The quantity $f(I)$ in Eq. (8) is the Debye-Hückel term, given by

$$f(I) = -\frac{4IA_\varphi}{b} \ln\left(1 + b\sqrt{I}\right). \quad (9b)$$

The variable $I = \frac{1}{2} \Sigma m_i z_i^2$ is the ionic strength, and coefficient values assigned by Pitzer[2] are $\alpha = 2.0$ and $b = 1.2$, valid for all electrolytes at any concentration or temperature. The Debye-Hückel coefficient A_φ is a function of temperature which is tabulated in Ref. 2.

Activity and osmotic coefficients are determined by differentiation of Eq. (8) as follows:

$$\varphi - 1 = -\frac{\partial}{\partial M_1}\left(\frac{G^{ex}}{RT}\right)\frac{1}{\Sigma m_i}$$
$$= \frac{2}{\Sigma m_i}\left\{-\frac{A_\varphi I^{3/2}}{1 + b\sqrt{I}} + m_2\sum_{j=3}^{6} m_j\left(B_{2j}^{\varphi} + ZC_{2j}\right) + \sum_{i=3}^{5}\sum_{j=i+1}^{6} m_i m_j\left(\Phi_{ij}^{\varphi} + m_2\psi_{2ij}\right)\right\} \quad (10)$$

$$\ln\gamma_2 = F(I) + \sum_{j=3}^{6} m_j\left(2B_{2j} + ZC_{2j}\right) + \sum_{i=3}^{5}\sum_{j=i+1}^{6} m_i m_j\psi_{2ij} + m_2\sum_{j=3}^{6} m_j C_{2j} \quad (11a)$$

$$\ln\gamma_j = z_j^2 F(I) + m_2\left(2B_{2j} + ZC_{2j}\right) + \sum_{\substack{i=3\\ i\neq j}}^{6} m_i(2\Phi_{ij} + m_2\psi_{2ij}) + |z_j| m_2\sum_{i=3}^{6} m_i C_{2i}\,, \quad (11b)$$
$$j = 3,4,5,6.$$

In the above equations,

$$Z = \sum_{i=2}^{6} m_i|z_i| \quad (12a)$$

$$B_{ij}^{\varphi} = \beta_{ij}^{(0)} + \beta_{ij}^{(1)}\exp\left(-\alpha\sqrt{I}\right) \quad (12b)$$

$$\Phi_{ij}^{\varphi} = \Phi_{ij} + I\Phi_{ij}' \quad (12c)$$

$$F(I) = -A_\varphi\left[\frac{\sqrt{I}}{1 + b\sqrt{I}} + \frac{2}{b}\ln\left(1 + b\sqrt{I}\right) + m_2\sum_{j=3}^{6} m_j B_{ij}' + \sum_{i=3}^{5}\sum_{j=i+1}^{6} m_i m_j\Phi_{ij}'\right] \quad (12d)$$

and the prime symbol (′) denotes differentiation with respect to ionic strength. The quantities Φ_{ij} describe interactions of like-charged ions, and can be represented as

$$\Phi_{ij} = \theta_{ij} + {}^{E}\theta_{ij}(I) \ . \tag{13}$$

If the two ions have the same charges (e.g., F^- and OH^-), then the ${}^{E}\theta = 0$ and Φ_{ij} is independent of ionic strength. However, for ions whose charges have the same sign, but different magnitude (e.g., OH^- and PO_4^{-3}), then ${}^{E}\theta_{ij}$ must be considered. The form for this function is discussed in Ref. 2, and considered further in Appendix B.

The parameters $\beta_{ij}^{(0)}$, $\beta_{ij}^{(1)}$, C_{ij}, θ_{ij}, and ψ_{ijk} must be determined empirically from data. One of the strengths of Pitzer's ion-interaction approach is that behavior of components in mixed solutions is largely determined by the binary parameters $\beta_{ij}^{(0)}$, $\beta_{ij}^{(1)}$, and C_{ij}, with the mixture coefficients θ_{ij} and ψ_{ijk} of secondary importance and significant only at higher ionic strengths. However, Harvie and coworkers[41] have noted the importance of these mixture quantities in accurately modeling phase equilibria (i.e., solubilities). Hence, initially θ_{ij} and ψ_{ijk} are assumed zero, but will be given non-zero values if data (especially solubility data) require it.

In order to cover a range of temperatures, the free energy functions $\hat{\mu}_i \equiv \mu_i^0/RT$ and binary Pitzer coefficients are considered to be functions of temperature of the form:

$$\hat{\mu}_i = \hat{\mu}_{i1} + \hat{\mu}_{i2}\left(T - T_0\right) + \hat{\mu}_{i3}\left(\frac{1}{T_0} - \frac{1}{T}\right) + \hat{\mu}_{i4}\ln\frac{T}{T_0} + \mu_{i5}\left(T^2 - T_0^2\right) . \tag{14}$$

Here, the first subscript refers to the species in question; the second refers to the particular temperature coefficient in Eq. (14). From Eq. (14), it is seen that $\hat{\mu}_i(T_0) = \hat{\mu}_{i1}$, where $T_0 = 298.15$ K throughout. This form is especially helpful, since there is usually

an abundance of data at 25 °C which can be used to determine $\hat{\mu}_{i1}$. Additional data at other temperatures can be used to determine one or more of the other parameters. Some of the temperature coefficients may be chosen to be zero, since it may be impossible to determine all of them with reasonable accuracy.

3.4 Calculation of Enthalpies

The dependence of activity coefficients on temperature can also be determined using enthalpy and heat capacity data. However, allowance must be made for the thermal effects on chemical reactions, such as the hydrolysis reaction (4). For situations which do not involve reaction, the analysis is much simpler. The following analysis considers TSP solutions with reaction (4) included. The application to simple binary systems such as Na-F and Na-HPO_4 are then derived from the more general equations.

Consider the dissolution of N_2 moles of pure anhydrous Na_3PO_4 into N_1 moles of water. The hydrolysis reaction will occur rapidly, so that the equilibrium system will contain n_i moles of the system constituents, where i is the species index from Eq. (7). Mass balances require that $n_2 = 3N_2$, $n_3 + n_4 = N_2$, $n_1 = N_1 - n_4$, $n_4 = n_5$. The total enthalpy change ΔH_{TOT} can be evaluated by considering the steps shown below:

(1) Solvation and dilution (to "infinite dilution"):

$$\infty\ H_2O\ +\ N_2\ Na_3PO_4\,(c) \rightarrow N_2\ Na_3PO_4\ (\infty\ H_2O), \qquad \Delta H_1 = N_2\,\Delta H_s^0 .$$

(2) Reaction at infinite dilution [cf. Eq. (4)]:

$$\Delta H_2 = n_4\ \Delta H_r^0 .$$

(3) Reconstitution of reacted system (water withdrawn until n_1 moles result):

$$\Delta H_3 = L(n_1,n_2,n_3,n_4,n_5) \; .$$

In step (1), water is added so that the N_2 moles of Na_3PO_4 (c) are at infinite dilution. The enthalpy change ΔH_s^0 represents the "molar heat of solution at infinite dilution" for the unhydrolyzed Na_3PO_4, and depends only on temperature. In step (2), $n_4 < N_2$ moles react at infinite dilution according to Eq. (4). The enthalpy change ΔH_r^0 is the standard molar heat of reaction (at infinite dilution). Various estimates are available, generally around 41 kJ/mol; however, in this case ΔH_r^0 will be determined by the optimization procedure. In step (3), water is withdrawn until the system reaches the actual equilibrium conditions, with the enthalpy change $L = H - H^0$. This term will be evaluated within the framework of the Pitzer ion-interaction treatment.

The total enthalpy change for the entire process is

$$\Delta H_{TOT} = \Delta H_1 + \Delta H_2 + \Delta H_3 = N_2 \Delta H_s^0 + n_4 \Delta H_r^0 + L \; .$$

Of particular importance is the apparent molar enthalpy related to the stoichiometric addition of Na_3PO_4:

$$L_{\varphi,TOT} = \frac{\Delta H_{TOT}}{N_2} = \Delta H_s^0 + \frac{n_4}{N_2} \Delta H_r^0 + \frac{L}{N_2} \; . \qquad (15)$$

Most data are given in terms of $L_{\varphi,TOT}$ since it is an easily measured quantity. For example, enthalpies of dilution involve two solutions with different constituent amounts.

Call them a (with N_2^a, N_1^a, n_i^a) and b (N_1^b, N_2^b, n_i^b). The enthalpy of dilution is then

$$\Delta H_{dil}(a \rightarrow b) = L_{\varphi,TOT}^{b} - L_{\varphi,TOT}^{a} = \left(\frac{n_4^b}{N_2^b} - \frac{n_4^a}{N_2^a} \right) \Delta H_r^0 + \left(\frac{L^b}{N_2^b} - \frac{L^a}{N_2^a} \right) . \quad (16)$$

Note that ΔH_s^0 drops out and is not involved in these calculations.

To calculate heats of reaction, recall that all free energies of formation are represented by Eq. (14). The free energy change for reaction (4) can then be represented by

$$\begin{aligned} \Delta\hat{\mu}_r &= \hat{\mu}_4 + \hat{\mu}_5 - \hat{\mu}_1 - \hat{\mu}_3 \\ &= \Delta\hat{\mu}_1 + \Delta\hat{\mu}_2(T - T_0) + \Delta\hat{\mu}_3\left(\frac{1}{T_0} - \frac{1}{T} \right) + \Delta\hat{\mu}_4 \ln\left(\frac{T}{T_0} \right) + \Delta\hat{\mu}_5(T^2 - T_0^2) , \end{aligned}$$

where

$$\Delta\hat{\mu}_1 \equiv \hat{\mu}_{41} + \hat{\mu}_{51} - \hat{\mu}_{11} - \hat{\mu}_{31}, \quad \Delta\hat{\mu}_2 \equiv \hat{\mu}_{42} + \hat{\mu}_{52} - \hat{\mu}_{12} - \hat{\mu}_{32}, \quad etc.$$

Note that for $\hat{\mu}_i$, the subscript refers to the species index, whereas for $\Delta\hat{\mu}_j$, the subscript denotes temperature coefficient. Application of the Gibbs-Helmholtz equation yields

$$-\frac{\Delta H_r^0}{RT^2} = \frac{\partial}{\partial T}\left(\Delta\hat{\mu}_r\right) = \Delta\hat{\mu}_2 + \frac{\Delta\hat{\mu}_3}{T^2} + \frac{\Delta\hat{\mu}_4}{T} + 2T\Delta\hat{\mu}_5$$

and thus

$$\Delta H_r^0 = -R\left(\Delta\hat{\mu}_2 T^2 + \Delta\hat{\mu}_3 + \Delta\hat{\mu}_4 T + 2\Delta\hat{\mu}_5 T^3\right). \quad (17)$$

As mentioned in Sect. 3.2, nominal values for coefficients in Eq. (14) have been determined by nonlinear least squares fitting to tabulated values from the HSC software.[39]

Values for water were obtained from the CODATA tables[38] and were fit to greater precision. The resulting coefficients are given in the first four rows of Table 5. Using Eq. (17), these values result in ΔH_r = 656 kJ/mol at 25 °C, clearly well off the accepted value of 41 kJ/mol. To rectify this problem, the coefficients for PO_4^{-3} and HPO_4^{-2} were recalculated, imposing the additional constraint of ΔH_r = 41 kJ/mol. The revised values are given in the last two rows of Table 5, and are very similar to the original values. Clearly the lower-order digits of each number are important for enthalpy determination, while perhaps not as important for other applications. The revised values were used as initial values in subsequent calculations, and the coefficients for HPO_4^{-2} were actually included as optimizable parameters. Thus, optimal values of ΔH_r^0 and of the equilibrium constant for Eq. (4) are end results of the current analysis.

Table 5. Temperature coefficients for free energies of formation

Species	Coefficients for Eq. (14)				
	$\hat{\mu}_1$	$\hat{\mu}_2$	$\hat{\mu}_3$	$\hat{\mu}_4$	$\hat{\mu}_5 \times 10^4$
H_2O	-95.665	-1.0029	0	324.040	5.0848
OH^-	-63.534	0.75606	0	0	-7.4688
PO_4^{-3}	-411.213	4.3353	0	0	-43.692
HPO_4^{-2}	-439.837	4.4361	0	0	-45.057
revised:					
PO_4^{-3}	-411.192	4.3307	0	0	-43.623
HPO_4^{-2}	-439.856	4.4422	0	0	-45.145

Solution enthalpy of the equilibrium solution is determined as

$$L = H - H^0 = -T^2 \frac{\partial}{\partial T}\left(\frac{G^{ex}}{T}\right)_{P,n_i},$$

where G^{ex} is given by Eq. (8). Performing this differentiation yields

$$\frac{-L}{M_1 RT^2} = \frac{\partial}{\partial T}\left(\frac{G^{ex}}{M_1 RT}\right)_{P,n_i} = -\frac{A_L I}{RT^2 b}\ln\left(1 + b\sqrt{I}\right) + 2m_2 \sum_{j=3}^{6} m_j\left(B_{2j}^{L} + m_2 C_{2j}^{L}\right), \quad (18)$$

where $A_L \equiv 4RT^2\, \partial A_\varphi/\partial T$

$$B_{ij}^{L} \equiv \frac{\partial B_{ij}}{\partial T} = \frac{\partial \beta_{ij}^{(0)}}{\partial T} + \frac{\partial \beta_{ij}^{(1)}}{\partial T} g(x),$$

$$C_{ij}^{L} \equiv \frac{\partial C_{ij}}{\partial T}.$$

and all mixture terms are assumed constant (that is, $\partial\Phi_{ij}/\partial T = \partial\psi_{ijk}/\partial T = 0$). This assumption holds throughout the remainder of this study, except in the case of like-charged ions where the magnitude of the charges are different. In this case, $\partial^E\theta/\partial T$ is not zero, and must be included. This term is evaluated in Appendix B, yielding a term which can be appended to the right-hand-side of Eq. (18).

It is helpful to rewrite Eq. (18) in terms of the association fraction $\alpha = n_4/N_2$, and the stoichiometric molality $m \equiv N_2/M_1 = N_2\Omega/n_1$. It then follows that the ionic strength is $I = 2m(3 - \alpha)$ and the equilibrium molalities can be represented as:

$$m_2 = \frac{3N_2}{M_1} = 3m, \quad m_3 = \frac{n_3}{M_1} = (1-\alpha)\frac{N_2}{M_1} = (1-\alpha)m, \quad m_4 = m_5 = \alpha m.$$

Substituting these definitions into Eq. (18) and rearranging, yields

$$L_\varphi = \frac{L}{mM_1}$$

$$= \frac{2(3-\alpha)A_L}{b}\ln\left(1+b\sqrt{I}\right) - 6RT^2 m\left[(1-\alpha)\left(B_{23}^L + 3mC_{23}^L\right) + \alpha\left(B_{24}^L + 3mC_{24}^L\right) + \alpha\left(B_{25}^L + 3mC_{25}^L\right)\right], \quad (19)$$

and this is precisely the last term of Eq. (15).

Note finally that the Pitzer Parameters $\beta_{ij}^{(0)}$, $\beta_{ij}^{(1)}$, and C_{ij} are temperature dependent quantities represented in the form of Eq. (14). Thus, the temperature derivatives are straightforward, and the temperature coefficients of these parameters are related to the dilution enthalpies of the total solution through Eqs. (16) and (19). A similar treatment can be performed for heat capacities. However, the manipulations become rather involved, and are therefore relegated to Appendix C.

In the case of simple binary solutions, Eqs. (15) and (16) can also be applied, with $\Delta H_r^0 = 0$. With no reaction, $\alpha = 0$ and the stoichiometric molality is equal to the actual molality. It is then possible to rewrite Eq. (19) in the general form[2] for a single cation *i* and anion *j*:

$$L_\varphi = \nu|z_i z_j|\frac{A_L}{2b}\ln\left(1 + b\sqrt{I}\right) - 2\nu_i\nu_j RT^2 m\left(B_{ij}^L + m\nu_i z_i C_{ij}^L\right), \quad (20)$$

where $\nu = \nu_i + \nu_j$, ν_i and ν_j being the stoichiometric coefficients of the ions in the dissolved solid.

SECTION 4

MODELING THE FLUORIDE-PHOSPHATE SYSTEM

The modeling tools developed in Section 3 are now combined with the data mentioned in Section 2. Preliminary to evaluating the full system (1), it is necessary to evaluate the various subsystems, Na–F–H_2O, Na–F–OH–H_2O, Na–HPO_4–H_2O, Na–PO_4–HPO_4–OH– H_2O. In each case, it is necessary to determine ion-interaction coefficients and free energies of formation as functions of temperature through the range 0-100°C, and hopefully, for ionic strengths of $I < 6$.

For Na-F and Na-HPO_4, it is reasonable to assume a binary system almost totally ionized. However, for systems involving PO_4^{-3}, there will either be substantial OH^- or HPO_4^{-2}, or both. In this case, the binary parameters for Na-PO_4 interactions must be evaluated from solutions which include other anions. This is not a trivial problem, and special care must be taken in evaluating data.

4.1 Parameter Estimation Process

For each subsystem, the process of fitting activity and free energy parameters goes through several stages, in order that good estimates be obtained before all parameters are optimized together. At each stage, values from previous stages are used but held constant, while new parameters are estimated using all data relevant to that

parameter. The final stage involves simultaneous refinement (optimization) of all parameters together, using as initial guesses those values obtained in previous stages.

The various stages used are as follows:

(1) Using binary data at 25°C, estimate binary parameters at 25°C.

(2) Using other binary data, estimate temperature coefficients of binary parameters.

(3) Using solubility data (and other mixture data, if available), estimate mixture parameters and free energies of formation (holding binary parameters constant).

(4) Include all data, refine estimates of all parameters simultaneously.

4.2 Results for Na-F Systems

From Fig. 1, in spite of the data scatter, it is clear that the solubility limit for binary NaF data is never far from 1 m. However, in mixed solutions, the ionic strength will easily exceed this value, and it is desired to model solutions up to $I = 6$ m. Extrapolation of NaF activity coefficient data this far is highly unreliable, but it is still necessary to have reasonable binary parameters in this range. In order to accomplish this, values for activity coefficients are estimated to 6 m by comparison with NaCl and NaBr data through this range. Selected values of this extension are included as actual data during stages (1) and (2), although they are given a high variance (i.e., low weight). Resulting parameter fits should not be expected to match this "data" closely. Data on NaCl and NaBr systems are available at 25°C, 0°C (freezing point depression), and 100°C (vapor pressure lowering), analogous to actual NaF data below 1 m. The estimated data is then omitted during the refinement stage (4), which involves mixture data at high ionic strengths.

Using these procedures, all relevant parameters have been determined and are listed in Table 6. The single subscripts indicate temperature coefficients in Eq. (14). When no subscript is given, the parameter is regarded as independent of temperature, and was determined using all available data, usually at more than one temperature.

Use of the parameters in Table 6 allows calculation of activities and phase equilibria in the Na-F subsystem, such as the solid solubility curve shown in Fig. 1. Unlike the fit of Linke,[3] the parameters used to produce this curve have been derived using solubilities of mixed systems as well as the binary system data. It appears in the figure to be a satisfactory representation.

Figures 3 and 4 depict the data and model calculations at 25 °C. Model prediction of both isopiestic results and e.m.f. results are somewhat low. In fact, there is some inconsistency in these sets of data — raising either calculated curve would force the other even lower. That is, bringing the calculated result closer to one set of data would take it even further from the other. Also shown in Fig. 4 are the added data points above the solubility limit — formed from comparison with NaCl and NaBr data. These points were used only in preliminary stages of the estimation process (i.e., stages 1 and 2). Recall that the final parameter estimates (stage 4) did not use this data, although the binary prediction is reasonably close anyway.

Model predictions of binary solution quantities are compared in Figs. 5-9 for temperatures other than 25 °C. Fig. 5 depicts freezing point depression data, consisting of osmotic coefficients derived using Eq. (2). Also shown are the estimated points at higher concentrations. The model calculation is somewhat lower than actual data, however, the

Table 6. NaF parameters

Parameters	Species	Value
$\hat{\mu}_1$	NaCl (s)	-155.003
$\hat{\mu}_2$	NaCl (s)	0.45193
$\hat{\mu}_1$	NaF (s)	-219.391
$\hat{\mu}_2$	NaF (s)	2.02
$\hat{\mu}_5$	NaF (s)	-0.0020871
C_p^0	Na^+, F^- (aq)	-88.4014
θ	Cl-F	-0.0164
θ	OH-F	0.1193
ψ	Na-Cl-F	-0.00045
ψ	Na-OH-F	-0.0350
$\beta_1^{(0)}$	Na-F	0.0330
$\beta_3^{(0)}$	Na-F	246.83
$\beta_4^{(0)}$	Na-F	-0.6728
$\beta_1^{(1)}$	Na-F	0.2456
$\beta_3^{(1)}$	Na-F	2833.0
$\beta_4^{(1)}$	Na-F	-9.451
C_1	Na-F	0.00281
C_3	Na-F	12.25
C_4	Na-F	-0.0436

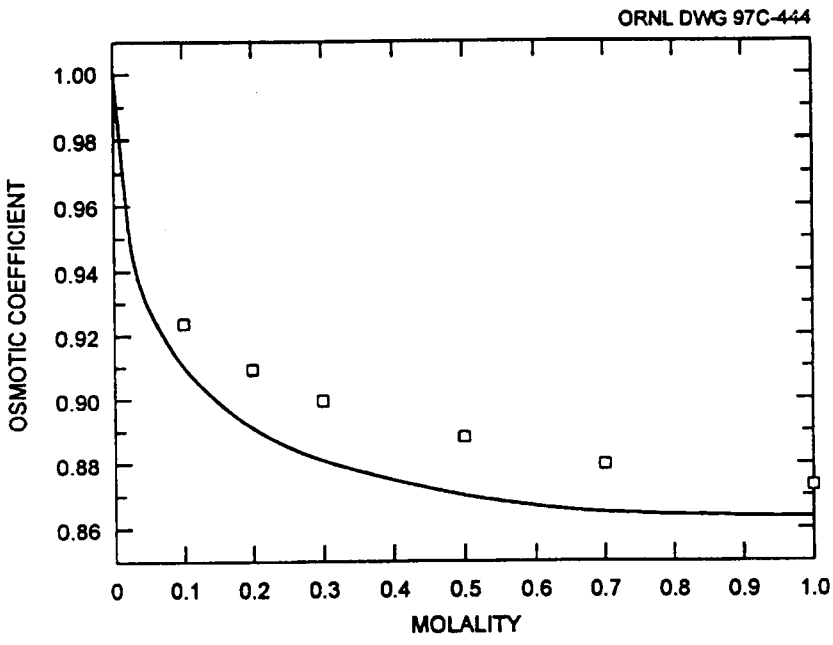

Figure 3. NaF isopiestic data at 25°C. □ Ref. 5, — this study.

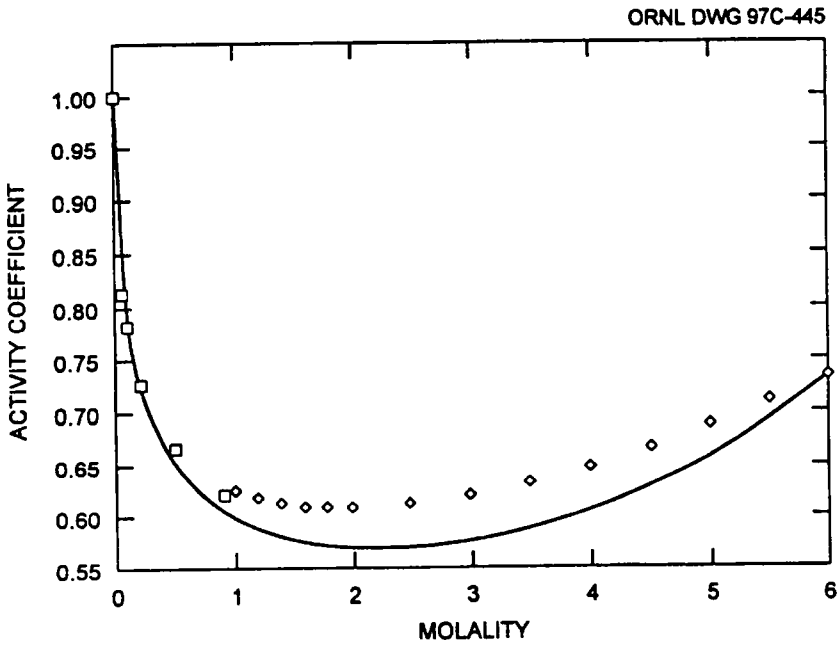

Figure 4. NaF e.m.f. data at 25°C. □ Ref. 6; ◊ estimated values (from comparison with NaCl and NaBr); — this study.

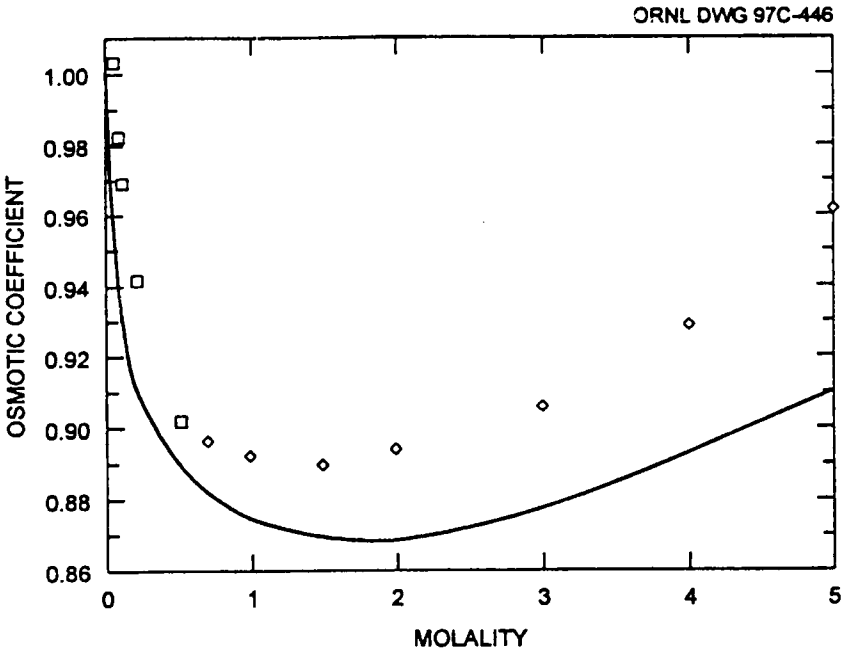

Figure 5. NaF freezing point depression data. □ Ref. 8, ◇ estimated values; — this study.

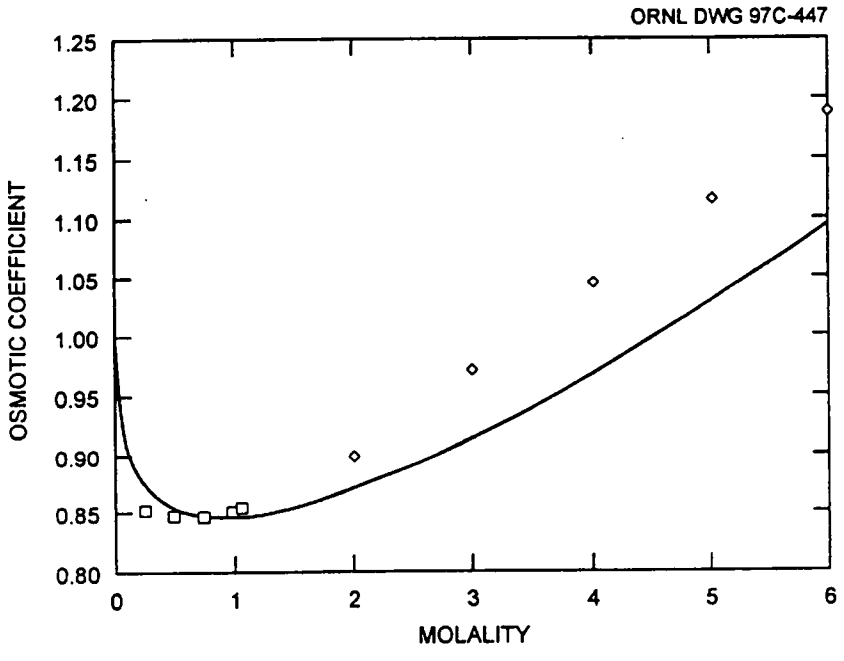

Figure 6. NaF vapor pressure data at 100°C. □ Ref. 9, ◇ estimated values; — this study.

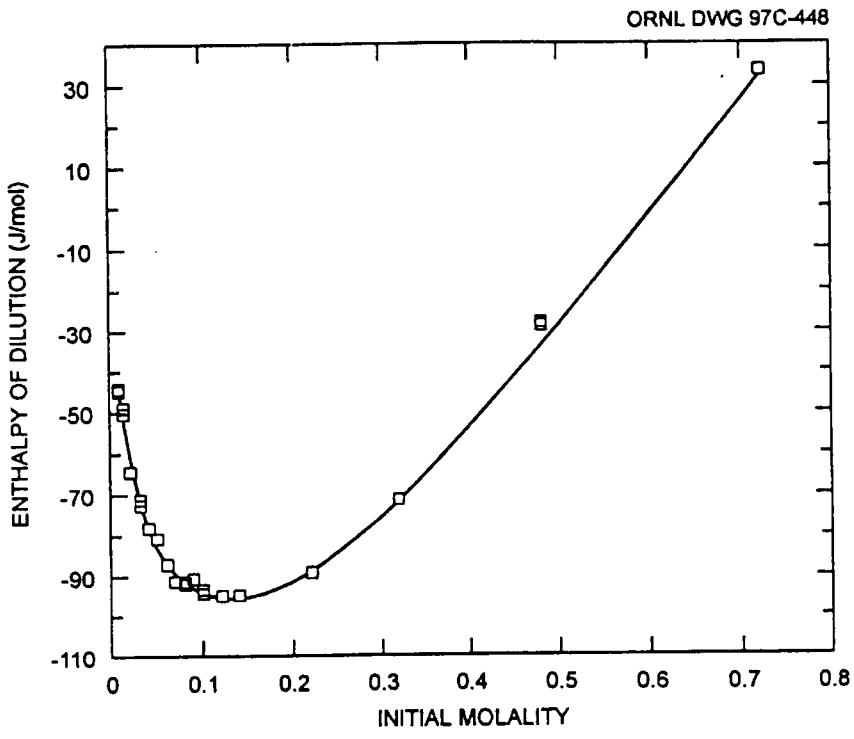

Figure 7. NaF enthalpies of dilution. □ Ref. 11, — this study.

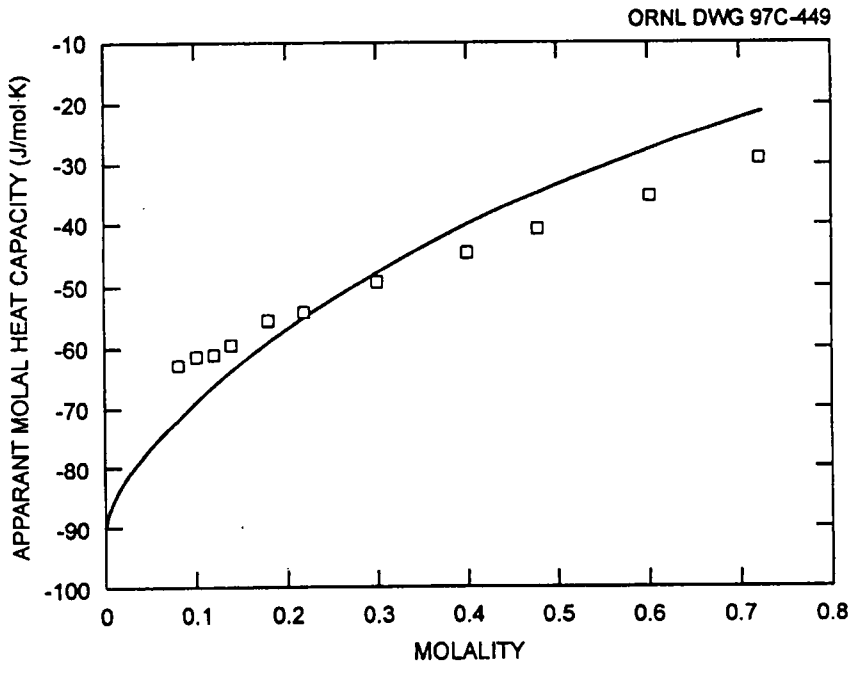

Figure 8. NaF heat capacity data. □ Ref. 11, — this study.

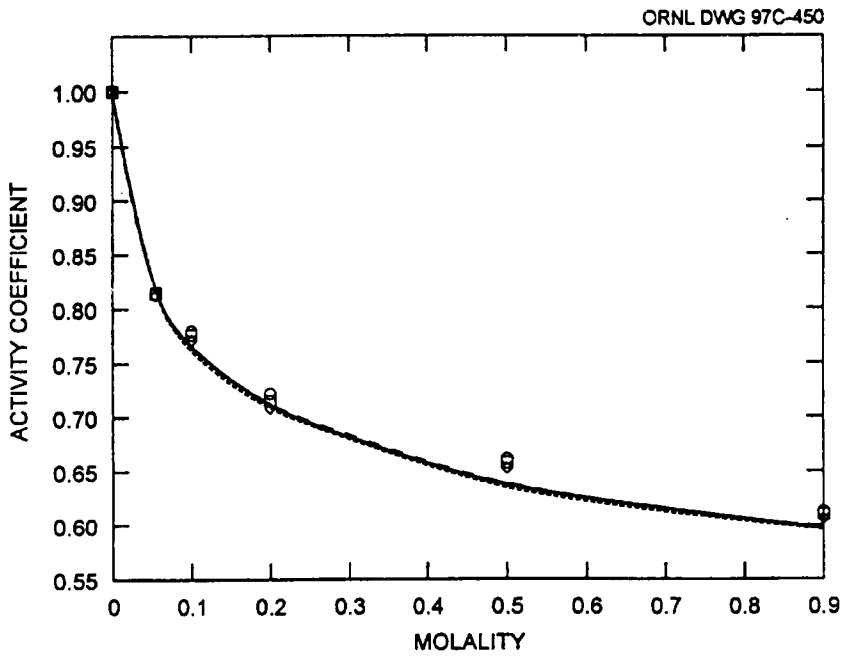

Figure 9. NaF e.m.f. data. Ref. 6: □ 15°C, ○ 25°C, ◇ 35°C, — this study.

data appears artificially high, even going above 1 at very dilute concentration. Thus, it is likely that the model is as good as the data — perhaps better.

Vapor pressure data at 100°C are shown in Fig. 6, together with the model calculation. There is good agreement with the actual data, although some discrepancy exists at low molalities. However, in this region the measurements are much more uncertain. As is the case with freezing point measurements, this data is quite old and may be suspect for that reason.

Much more recent data are available for other thermodynamic quantities, shown in Figs. 7 and 8. Model calculations closely match the dilution enthalpy measurements, and give a reasonably good prediction of the heat capacity. In the former case, the initial

concentration was exactly twice the final value for each pair, making it possible to compare results as a function of concentration.

The final set of binary system data is a comparison of e.m.f. data at 15°, 25°, and 35°C (the values at 25°C are also shown in Fig. 4). As seen in Fig. 8, there is very little change in activity coefficients due to temperature, in either the data or the model calculations. The model is, however, slightly low in each case.

Solubilities in mixed systems are shown in Figs. 10-13. For Na-Cl-F at (Figs. 10 and 11), agreement with the data is quite good, showing a decrease in NaF solubility as NaCl is added. In the vicinity of 6 m NaCl, an invariant point is reached which appears as a corner on the computed curve. Both the curve and data continue sharply downward, indicating a region of NaCl precipitation. In Fig. 10, the data of Campbell[14] match closely the calculated results for concentrations $m < 2$, but are quite inconsistent with all other data (and the calculated solubilities) at high molalities. For this reason, this data set was not included in the optimization process.

Solubilities in Na-Cl-F solutions are very nearly identical at 35°C and 50°C, as seen in Fig. 11. The model calculations are quite consistent with data in this regard. They are also consistent with the binary solubilities (Fig. 1) and the activity data (Fig. 8), which indicate only slight temperature effects.

For Na-OH-F systems, the results in Fig. 12 also show very slight temperature effects. Only at 20°C does the data extend to high concentrations, and the model prediction matches the data fairly well. Data at 0, 20, 40, 80, and 94°C are compared with the model predictions in Fig. 13. A perfect match would lie on the diagonal line. The model gives a reasonably good fit, at least within the uncertainty of the data.

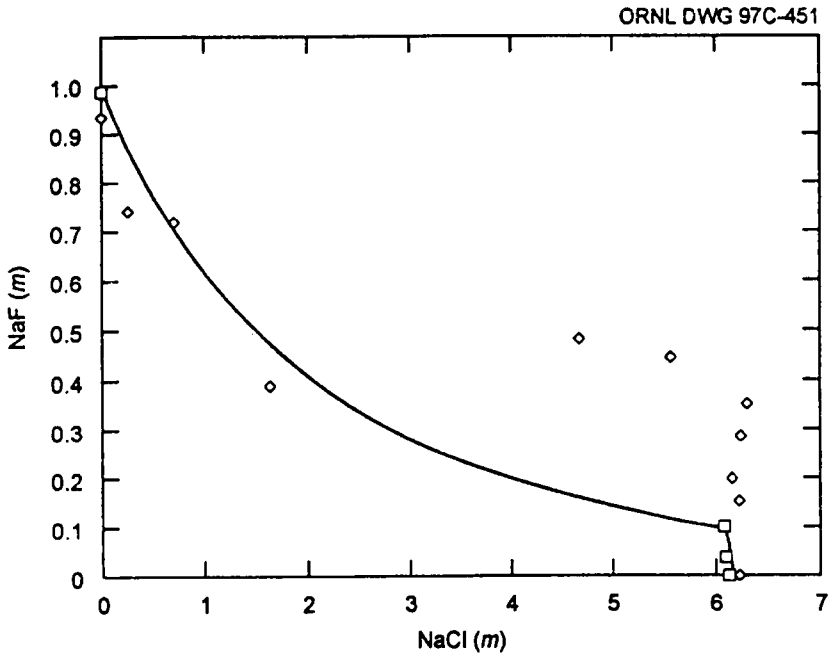

Figure 10. Solubility in the ternary system Na-Cl-F at 25°C
□ Ref. 12, ◇ Ref. 14, — this study.

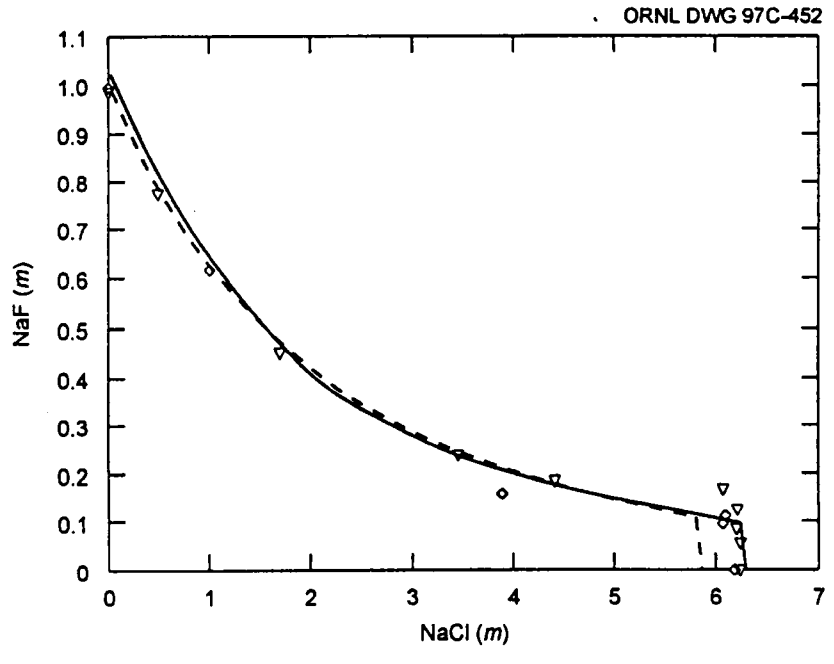

Figure 11. Solubility in the ternary system Na-Cl-F above 25°C.
◇ Ref. 12 (35°C), ▽ Ref. 13 (50°C), --- this study at 35°C,
— this study at 50°C.

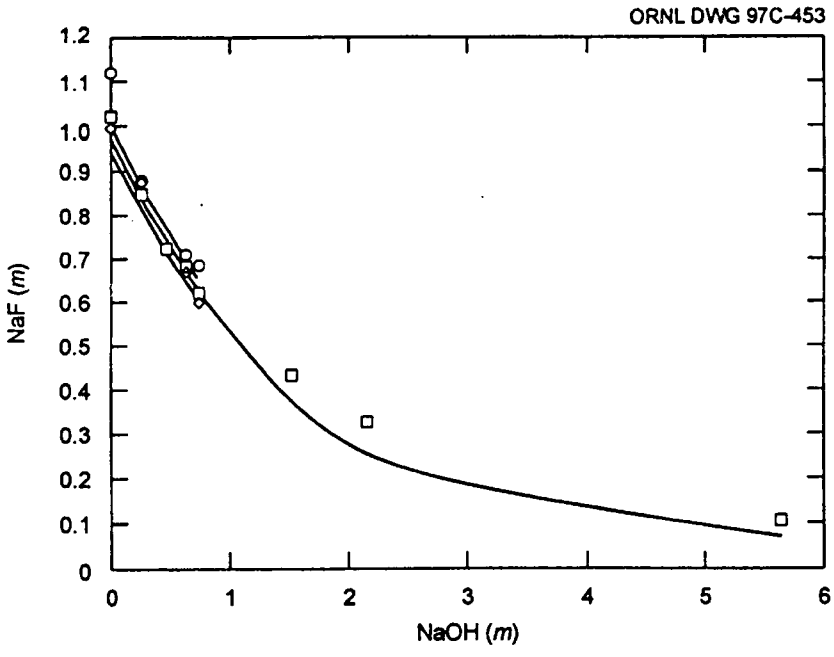

Figure 12. Solubility in the ternary system Na-OH-F. ◊ 0°C, □ 20°C, ○ 40°C, Ref. 15, — this study.

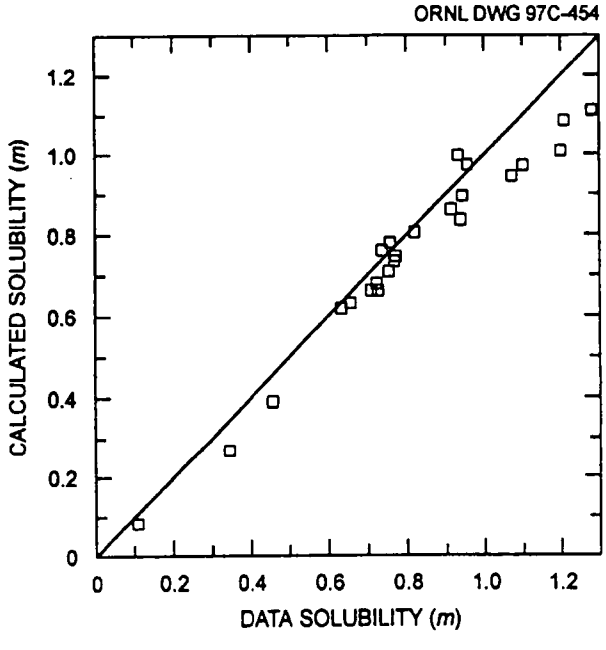

Figure 13. Comparison of calculated and measured solubility data for the Na-OH-F system (0–94°C). Data from Ref. 15.

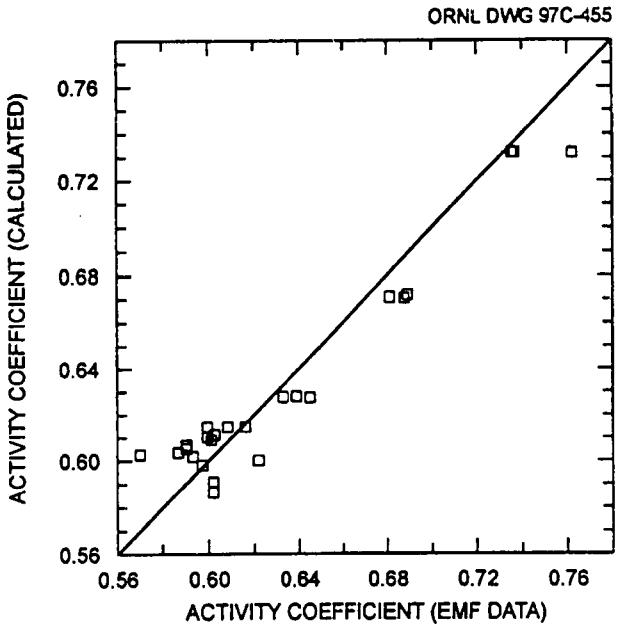

Figure 14. Comparison of calculated and measured NaF activity coefficients in the system Na-Cl-F at 25 °C. Data from Ref. 16.

Finally, Fig. 14 illustrates e.m.f. data in mixed Na-Cl-F solutions at 25 °C, presented in the same format as Fig. 13. The model calculations match the data within the uncertainty of the data.

4.3 Results for Na-HPO_4

Using only the isopiestic data of Refs. 17 and 18, parameters at 25 °C were determined with excellent precision. Following this, temperature coefficients were determined by fitting to all other data, while holding constant the values at 25 °C. The parameters resulting from these two steps are given in Table 7. The refining step yielded values which differed very little from those already determined, and so the latter were

Table 7. Parameter estimation for Na_2HPO_4

Parameter	Value
$\beta_1^{(0)}$	-0.03045
$\beta_3^{(0)}$	1826.0
$\beta_4^{(0)}$	-5.159
$\beta_1^{(1)}$	1.3504
$\beta_3^{(1)}$	6023.0
$\beta_4^{(1)}$	-18.774
C_1	0.00359
C_3	-282.6
C_4	0.8267
C_p^0	-209.3

regarded as sufficient. (Note that no mixture data is involved for this system, so that stage (3) is omitted.)

These model parameters are capable of representing most of the data quite well, as shown in Figures 15-19. Excellent agreement is obtained with the isopiestic data at 25°C (Fig. 15), the freezing point results (Fig. 16), the dilution enthalpies (Fig. 17), and the vapor pressure data at 100°C (Fig. 18). Regarding the latter, only the values for $m \leq 4$ were used in the optimization process, so it is not surprising that the calculated curve departs from data for $m > 4$. There is a slight discrepancy between the heat capacity data and the calculation at low m (Fig. 19). However, it should be remembered that these data were extrapolated from mixed solution data and heat

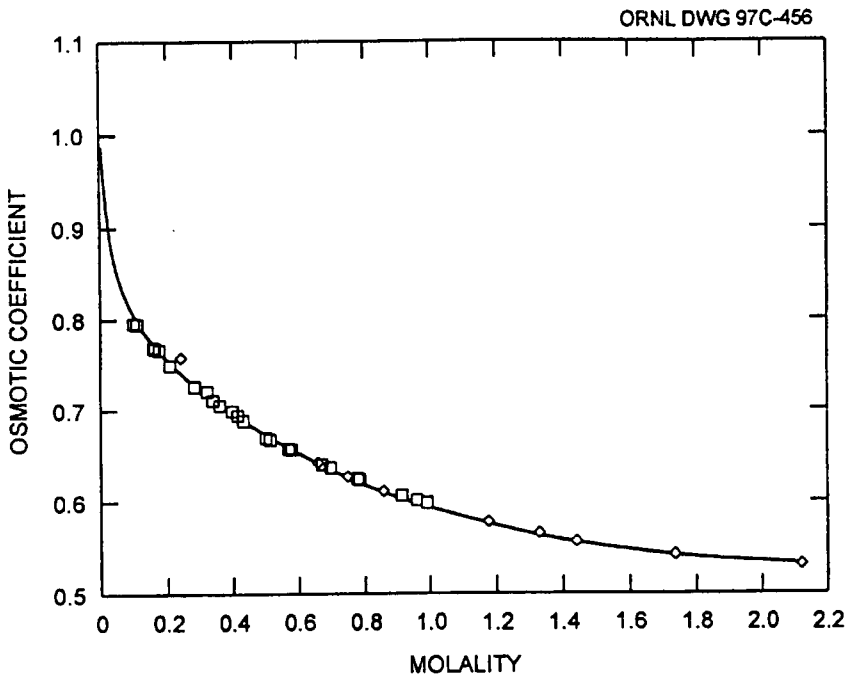

Figure 15. Na_2HPO_4 isopiestic data at 25°C. □ Ref. 18, ◇ Ref. 17, — this study.

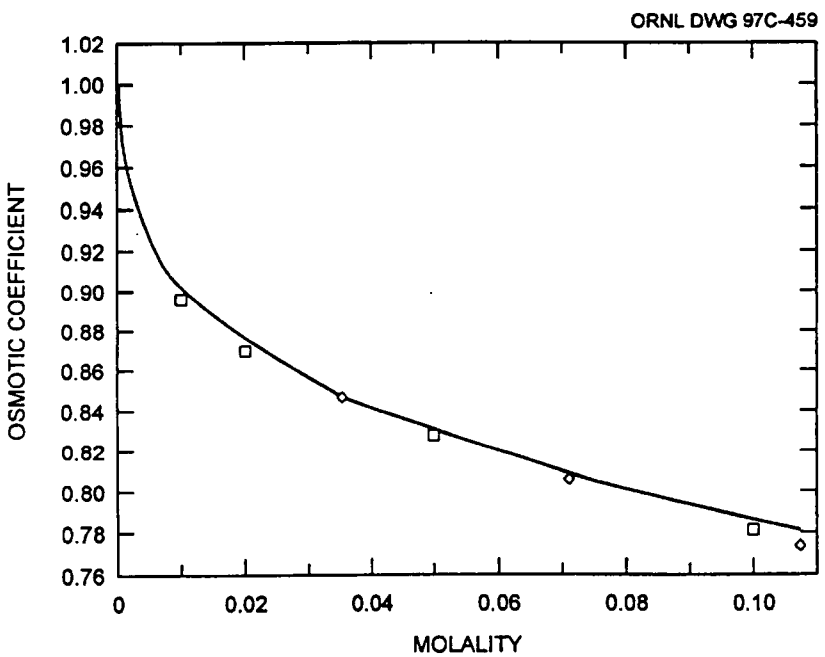

Figure 16. Na_2HPO_4 freezing point depression data. □ Ref. 23, ◇ Ref. 22, — this study.

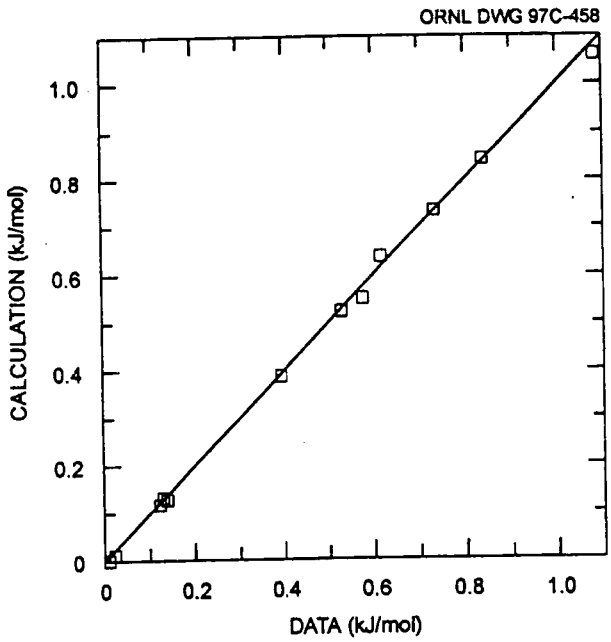

Figure 17. Comparison of calculated and measured values for Na_2HPO_4 dilution enthalpies. Data from Ref. 19.

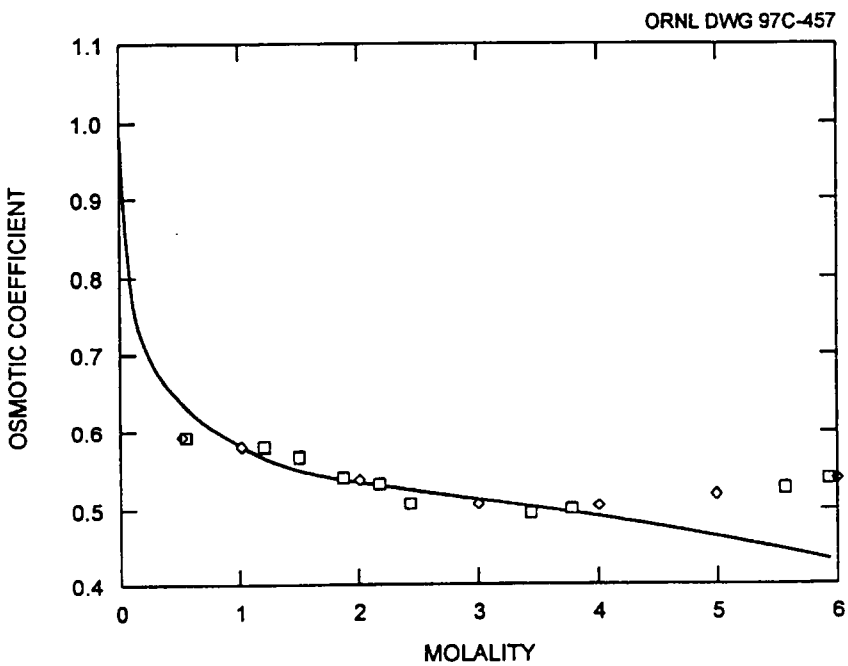

Figure 18. Na_2HPO_4 vapor pressure data at 100°C. □ Ref. 24, ◇ Ref. 25, — this study.

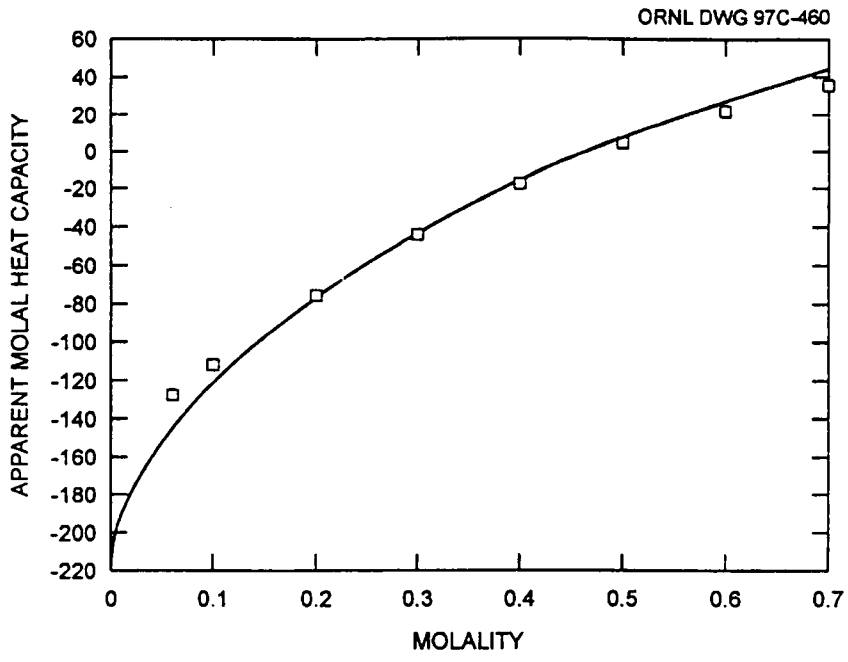

Figure 19. Na_2HPO_4 heat capacity data. □ Extrapolated values from Refs. 20 and 21, — this study.

capacity data at low concentrations is generally quite uncertain. In general, this fit is also quite good.

4.4 Results for Na-PO_4

The data in Table 3 were used to estimate values for all parameters that describe aqueous TSP solutions. Initially all unknown mixture parameters were assumed to be zero, and the sequence in Section 4.1 yielded excellent fits to the binary parameters [stages (1) and (2)], fair predictions of solubility at 0, 25 and 40°C, but poor results at 60°C. Trial-and-error choices of mixture parameters greatly improved solubility results at all temperatures. However, the nonzero mixture parameters did slightly affect the estimation of binary parameters. Hence, for each choice of mixture parameters, the

entire sequence of stages in Section 4.1 needed to be taken. After several such trials, the choice of $\theta(OH, PO_4) = 0.1$ and $\psi(Na,OH,PO_4) = 0.03$ gave excellent solubility results without compromising the estimation of binary parameters. The entire list of parameters determined in this process is shown in Table 8.

Figures 20-28 illustrate model recalculations using these parameters and compare them with the actual data used. In general, the model calculation fits the highest quality data best, due both to the inherent compatibility and the greater weighting of this data during parameter estimation. For example, the model prediction of isopiestic data (Fig. 20) and dilution enthalpies (Fig. 23) is excellent. Correspondence of data and calculation for freezing point depression (Fig. 21) and vapor pressure at 100°C (Fig. 22) is good, although accuracy begins to lag as concentration increases. Heat capacity predictions (Fig. 24) reproduce the data used (from Ref. 25) at least as well as other measurements (i.e., those of Ref. 26).

Prediction of phosphate solubilities is also quite good, as indicated in Figs. 25-28. At 25°C, model prediction of TSP is excellent through the entire range of data. Especially noteworthy is the region of high phosphate in Fig. 25, where prediction curves of TSP and disodium phosphate (DSP, $Na_2HPO_4 \cdot 12\ H_2O$) meet at the invariant point on the far right. The calculated curve also matches data fairly well in the region of high excess hydroxide, where the curve is nearly vertical. However, there does appear to be a slight systematic deviation, with the calculation underpredicting the data. In certain applications, it may be expedient to improve the prediction in this region, which can be accomplished by neglecting the other portion. If the value $\mu_1(TSP) = -1927.4$ in

Table 8. Optimal parameter values for trisodium phosphate systems

Parameter	Species	Coefficients[a]				
		1	2	3	4	5
$\beta^{(0)}$	Na-PO_4	0.2534	0	130.33	0.1247	0
$\beta^{(1)}$	Na-PO_4	3.7384	0	23820	–70.366	0
C	Na-PO_4	–0.02260	0	0	–0.00016	0
θ	OH-PO_4	0.1	0	0	0	0
ψ	Na-OH-PO_4	0.03	0	0	0	0
$\hat{\mu}$	HPO_4^{-2}(aq)	–439.592	4.74018	0	0	–0.00499766
$\hat{\mu}$	TSP(s)	–1927.400	–1350.9963	–4.1882317	415.57092	–731.17129
$\hat{\mu}$	DSP(s)[b]	–1803.470	7.65392	0	0	0
C_p^0	solution	–507.7				

[a]Each parameter is determined by the functional form of Eq. (14); the column headings denote subscripts for temperature coefficients.

[b]Disodium phosphate dodecahydrate $Na_2HPO_4 \cdot 12\ H_2O$.

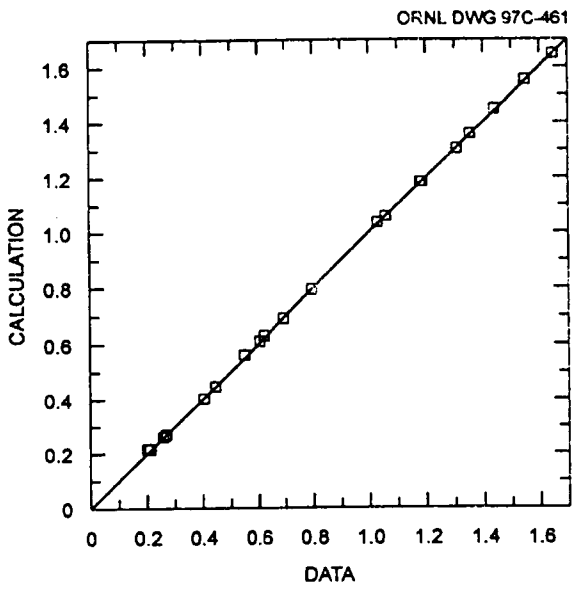

Figure 20. Comparison of calculations and isopiestic data for Na_2HPO_4/Na_3PO_4 buffer solutions at 25°C. Data from Ref. 18.

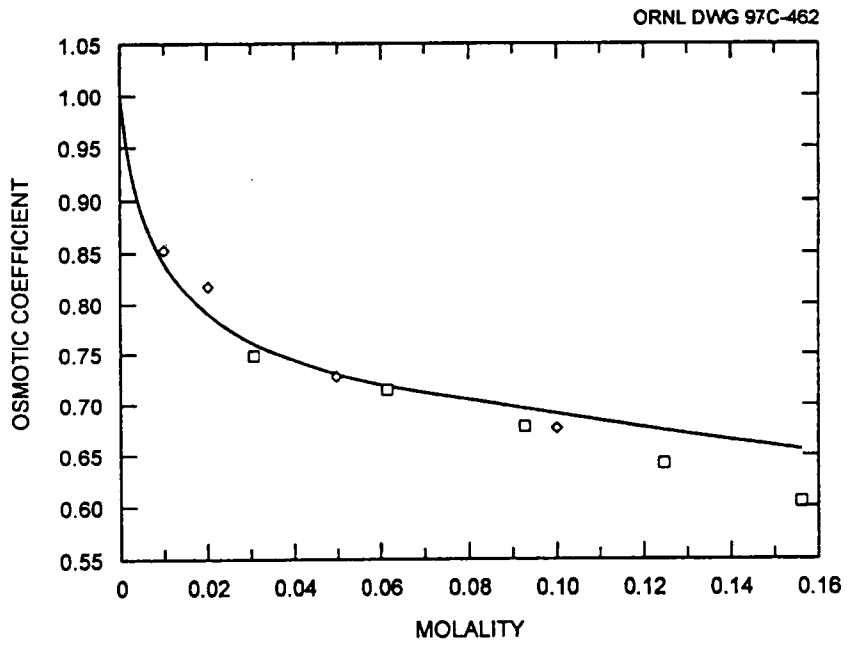

Figure 21. Na_3PO_4 freezing point depression data. □ Ref. 22, ◇ Ref. 23, — this study.

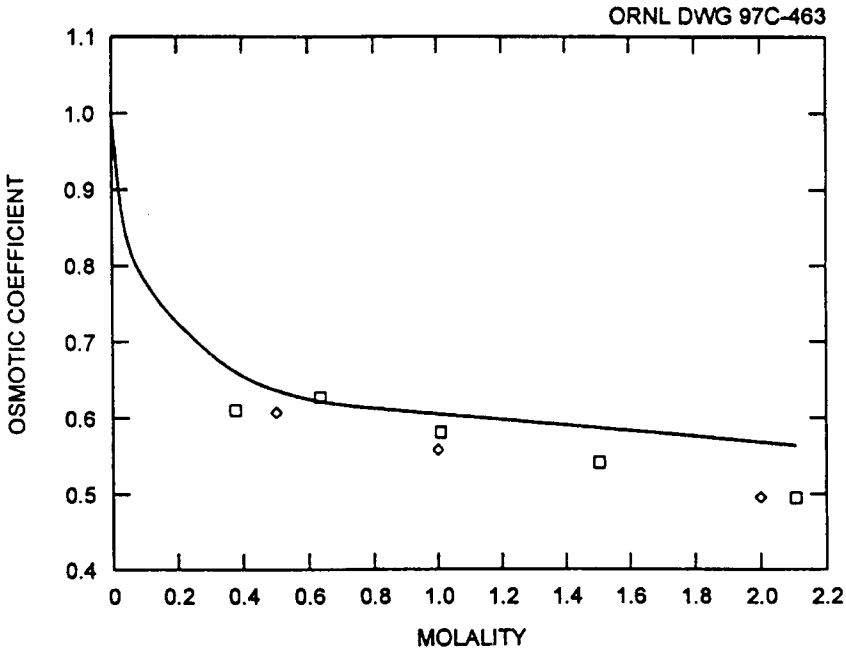

Figure 22. Na_3PO_4 vapor pressure data at 100°C. □ Ref. 24, ◇ Ref. 25, — this study.

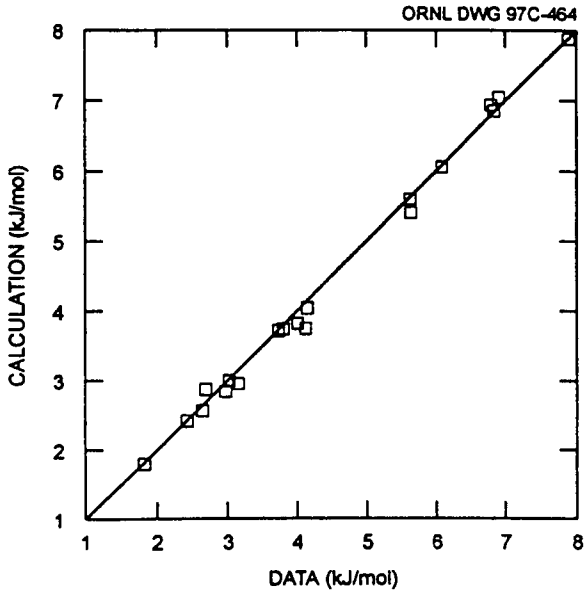

Figure 23. Comparison of calculated and measured values of dilution enthalpies for Na_3PO_4 at 25°C. Data from Ref. 19.

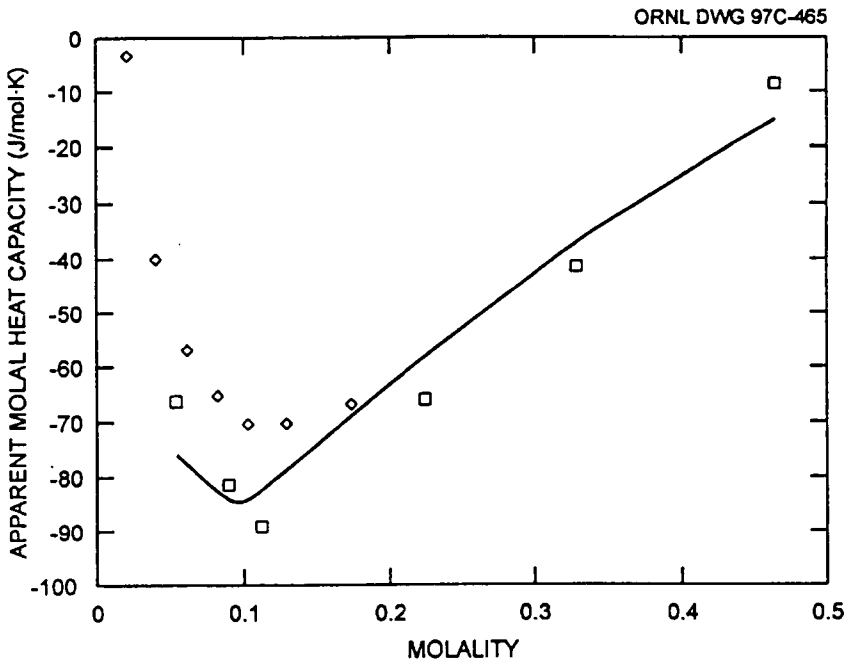

Figure 24. Na_3PO_4 heat capacity data at 25°C. □ Ref. 20, ◇ Ref. 21 (not used), — this study.

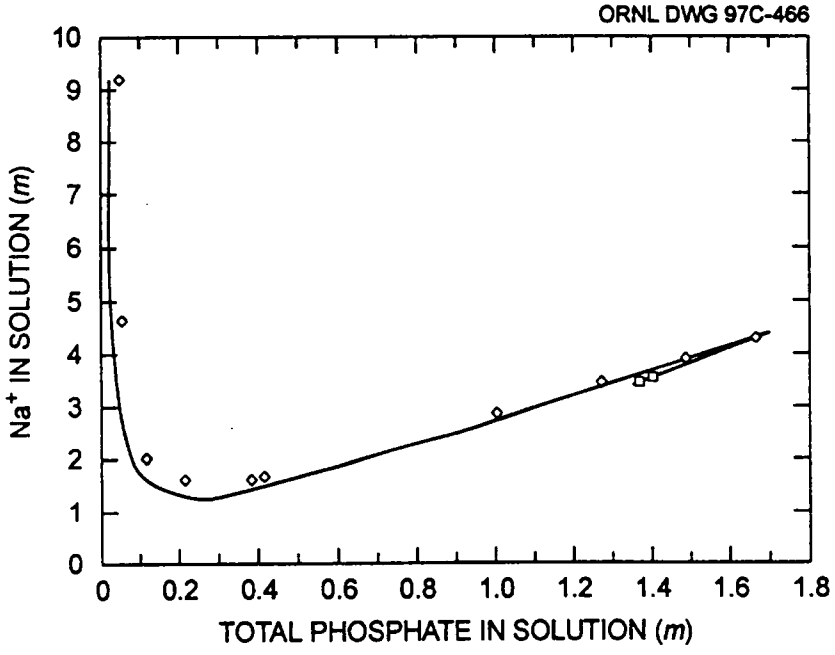

Figure 25. Phosphate solubilities in Na-PO_4-OH systems at 25°C. ◇ TSP and □ DSP from Ref. 26, — this study.

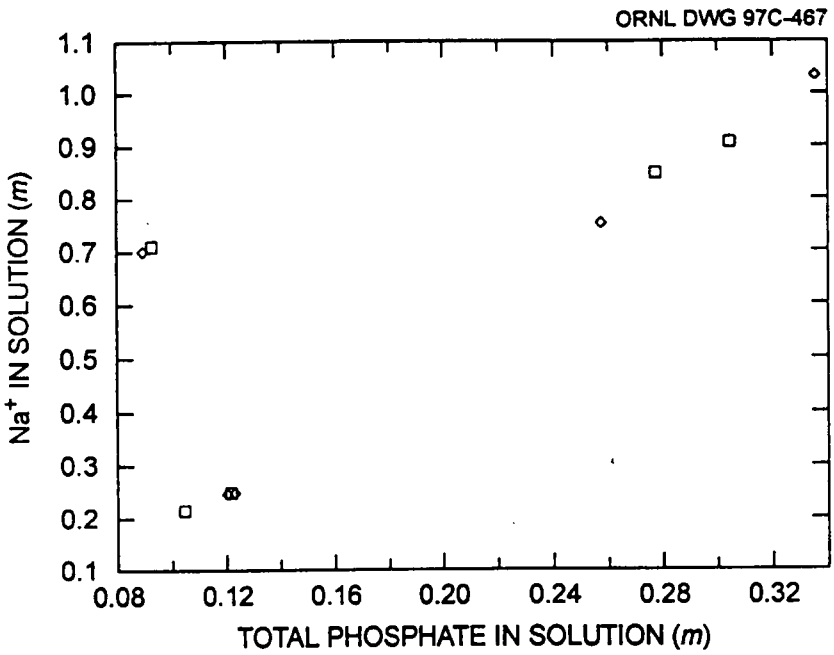

Figure 26. Phosphate solubilities in the system Na-PO_4-OH at 0°C. ◇ Ref. 26, □ this study.

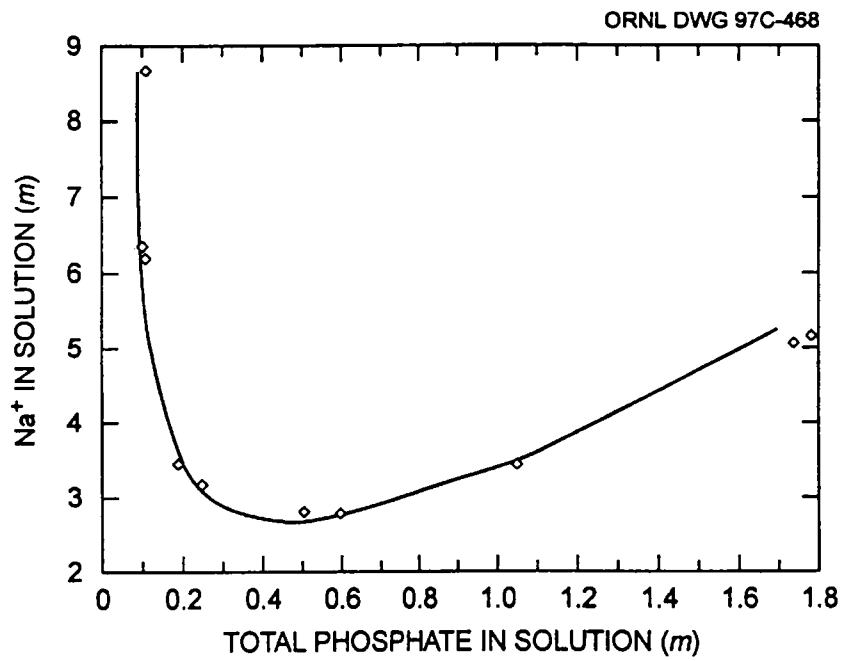

Figure 27. Phosphate solubility in the Na-PO_4-OH system at 40°C. ◇ Ref. 26, — this study.

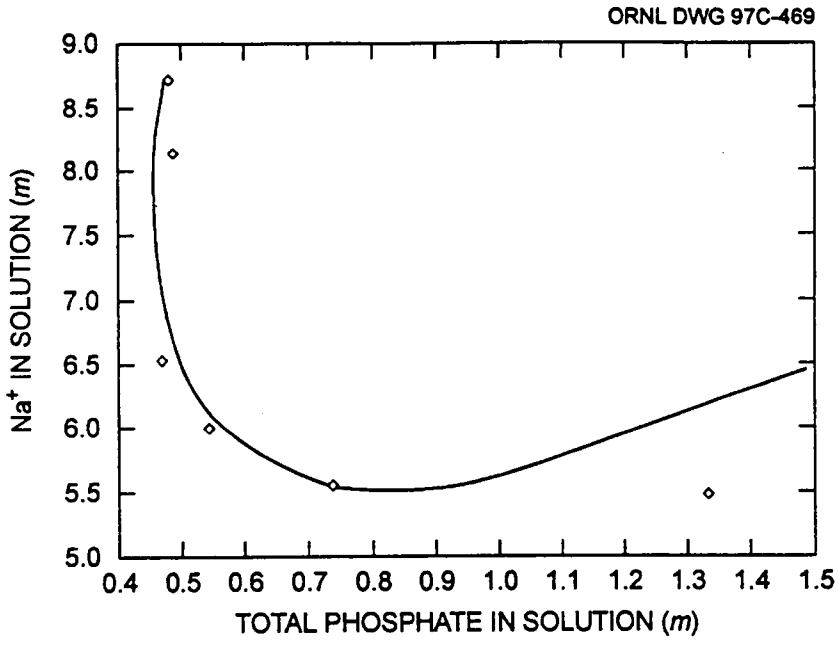

Figure 28. Phosphate solubility in the Na-PO_4-OH system at 60°C.
◇ Ref. 26, — this study.

Table 8 is raised to –1926.923, then the solubility of TSP is raised sufficiently to provide an excellent match of data out to 1 m PO_4^{-3}. However, as phosphate increases above 1 m, deviation becomes significant, and the invariant point is missed entirely (i.e., the curves for TSP and DSP never do meet). Thus, for high caustic applications near 25°C, the alternate value could prove useful, but it does not cover the whole range of TSP solubility.

At 0°C, prediction and data are hard to compare, since the paucity of data precludes formation of a noticeable curve or pattern. The model does match data adequately, as shown in Fig. 26, for both TSP and DSP.

Depicted in Figs. 27-28 are predictions of TSP solubility at 40°C and 60°C, which compare very well with data. The main failure is for high phosphate

concentrations at 60°, in which the model curve clearly overpredicts the lone data point. In addition, at low phosphate concentration (Fig. 28), the nearly vertical portion of the computed curve shows somewhat more curvature than is suggested by the data. These problems could be remedied by using temperature dependent values for the mixture parameters θ and ψ, however the small amount of data hardly warrants it. In general, the model will be applied primarily to regions of moderate phosphate (below 1 m) and high caustic (up to 6 m OH^-). In this region, clearly model prediction of data is quite good.

4.5 Fluoride-Phosphate Systems

The data at 25°C from Refs. 27 and 28 were used to determine the mixture parameter $\theta(F,PO_4)$ and the nominal value of $\hat{\mu}$ (DS). Fig. 29 shows each data point, linked by a straight line to the corresponding calculated point. (Since the hydroxide concentration varies, it is not useful to try to connect the data points together with a curve.) While there are discrepancies, the horizontal nature of the longest lines indicates that most serious errors are between calculated and measured fluoride values. This is borne out in Fig. 30, where calculated and measured phosphate values are compared. The diagonal line denotes a perfect match, and the plot indicates reasonable agreement between data and calculated values. A similar plot of fluoride data does not indicate such good agreement. For this reason, all fluoride measurements are considered more uncertain; hence, the data were re-weighted and fit again.

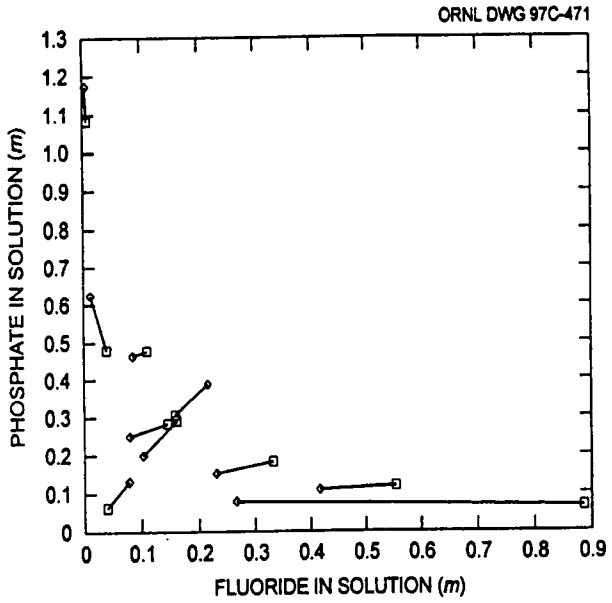

Figure 29. Solubilities in the Na-F-PO_4-OH system at 25°C. ◇ Data from Refs. 27 and 28, □ calculation.

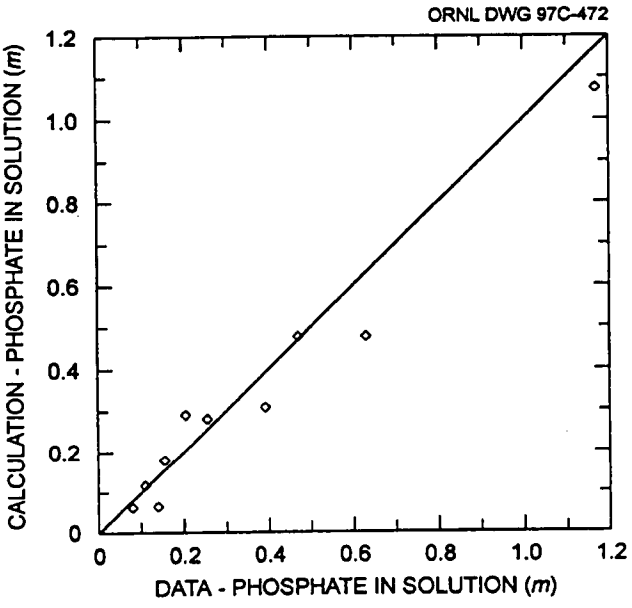

Figure 30. Comparison of calculated and measured phosphate in solution for the Na-F-PO_4-OH system at 25°C. Data from Refs. 27 and 28.

Table 9. Fluoride-phosphate optimal parameters

Parameter	Species	Value
$\hat{\mu}_1$	DS	-3512.445
$\hat{\mu}_2$	DS	36.15256
$\hat{\mu}_5$	DS	-0.0377395
θ	F-PO_4	0.5513

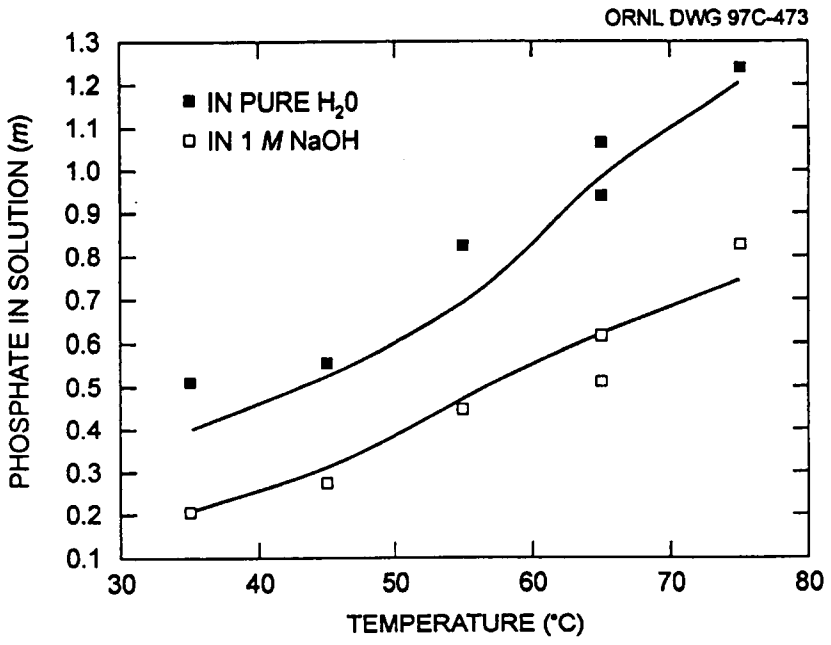

Figure 31. Solubility of the double salt between 35-75 °C. ■ pure H_2O and □ 1 M NaOH from Ref. 28, — this study.

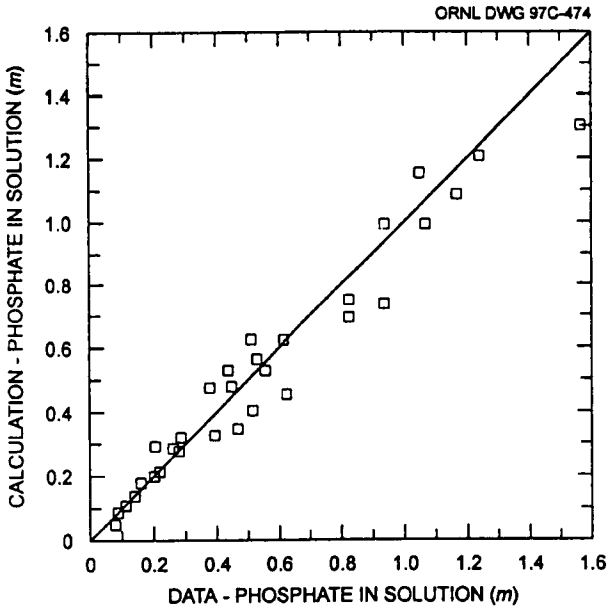

Figure 32. Comparison of calculated and measured values for the Na-F-PO_4-OH system at 25–100°C. Data from Refs. 27, 28, and 30.

Data points at temperatures other than 25°C were used to fit temperature coefficients for $\hat{\mu}$ (DS), assuming the mixture parameter θ was constant. The resulting optimal parameter values are given in Table 9, and were used to recalculate solubilities, which are compared with data at many temperatures in Figs. 31-32. It can be seen in the figures that there is reasonable agreement between the two. It should be noted that only one additional mixture parameter was needed to fit the available data. Perhaps with additional data, the parameter ψ(Na, F, PO_4) would also be needed.

SECTION 5

EXPERIMENTAL VERIFICATION

The purpose of this section is to verify the predictive capability of a model formed by combining all results from previous sections. The data used in this section are from new experiments or from sources not used in the actual parameter estimation process, since they are not as quantitative as data mentioned in Section 2. However, they do lend themselves to qualitative comparison over a wide range of conditions, including extrapolations outside the range of data used in parameter estimation. In Section 5.1, various estimates are given for the equilibrium constant of the hydrolysis reaction (4). In Section 5.2, additional solubility data is obtained as a part of this study, to better understand the fluoride-phosphate system.

Collecting all parameters from Tables 6–9 and using them as input to the equilibrium calculation represents a comprehensive model of sodium-fluoride-phosphate behavior. Of course, calculations using such a model are only so good as the data used to fit parameters. Since data at 25 °C are usually of superior quality, we expect model predictions at this temperature to be reasonably accurate. However, as temperatures vary away from 25 °C, data are increasingly sparse and uncertain; hence, model predictions are likewise more uncertain.

The same can be said for concentration range. The Pitzer model was designed for moderate ionic strengths, $I \leq 4$, although extension to $I = 6$ is usually quite

acceptable. In some cases, extension to $I = 9$ or 10 is also possible, although somewhat less trustworthy. Thus, the prediction of TSP solubilities at 40°C and 60°C, up to $I = 9$ (cf. Figs. 27-28) was stretching the method to the limits of its ability.

5.1 Phosphate Hydrolysis Equilibrium

The hydrolysis reaction (4) can be characterized by properties such as equilibrium constant and heat of reaction. Such quantities could have been included as additional data in the parameter estimation process. However, they generally occur only at 25°C, and would have added very little to the data available at that temperature. In addition, measurements are usually made on systems of KCl or NaCl containing quite small amounts of phosphate (usually around 0.01 m, and often not stated), whereas the motivation for this work requires understanding systems with phosphate inventories as high as 1 m. Thus, except for the heats of reaction used to revise free energy estimates in Table 5, this data has been largely ignored.

However, it is useful now to check model predictions by comparison with data for reaction (4). From the temperature coefficients of free energy, the heat of reaction can be determined as a function of temperature from Eq. (17). The coefficients for HPO_4^{-2} were optimized in this study, and the resulting heat of reaction is shown in Fig. 33, along with various estimates from other researchers. The data at 25°C from Pitzer,[42] Christensen,[43] Irani and Taulli,[44] and at 30°C from Millero[19] were all obtained from calorimetric measurements. The value of Daniele[45] is obtained from the temperature dependence of the equilibrium constant, using data at 0, 10, 20, 30, 40, and

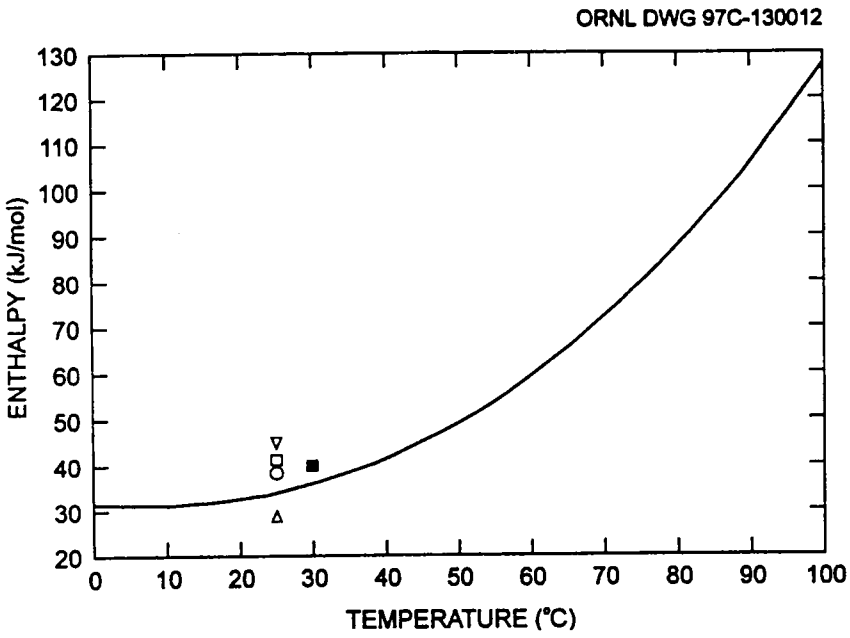

Figure 33. Enthalpy of reaction for phosphate hydrolysis. □ Ref. 42, ○ Ref. 43, ▽ Ref. 44, △ Ref. 45, ■ Ref. 19, — this study.

50°C. The latter approach introduces error through the differentiation of a function known only approximately, which can be a very unstable process. However, in the case of Daniele et al.,[45] there is sufficient data so that this effect is probably not dominant. The calorimetric data generally involve heats of dilution, and a primary source of error is extrapolation to zero ionic strength. Data from very dilute solutions are more useful in the extrapolation, but also have higher measurement uncertainty. Hence, this approach can also be somewhat inaccurate.

In the present study, both calorimetric and activity data were used; hence, the resulting heat of reaction involves both. It should not be surprising then that the estimate of this work lies between other estimates. As seen in Fig. 33, it is somewhat

below estimates based purely on calorimetry, and above that based solely on temperature dependence of the equilibrium constant.

Most estimates of equilibrium constants for reaction (4) have involved trace amounts of phosphate in NaCl or KCl solutions. The equilibrium quotient is formulated based on concentrations (rather than activities):

$$Q = \frac{m_4 \, m_5}{m_3}$$

Extrapolation of the quotient to zero ionic strength yields the equilibrium constant, since activities become equal to concentrations in this limit.

The prediction of equilibrium quotients using the present model is compared to data in Figs. 34 and 35. In each case, the model assumed 0.01 m total phosphate in NaCl solution. At 25°C the prediction matches data of Daniele[45] and Hershey[46] fairly well out to 3 m. It is in excellent agreement with the widely accepted equilibrium constant of Vanderzee and Quist.[47] (The current model predicts $\log_{10} K = 1.63$, whereas the value from Ref. 47 extrapolates to 1.62.) At 50°C, Fig. 35 shows that the model prediction lies between the data of Daniele[45] and Mesmer and Baes.[48] The latter used solutions of KCl, which could not be described exactly in the present model. These researchers also include two data points at 100°C, which are also underpredicted by the model, as stated in Table 10. The discrepancy may indicate error in model or data, but cannot be further resolved unless K^+ is included in the model.

Finally, the association fraction $\alpha = m_4/(m_3 + m_4)$ is plotted for various total concentrations in Fig. 36. Initially, all phosphate was input as anhydrous Na_3PO_4. For dilute solutions, HPO_4^{-2} is the dominant species at high temperatures (i.e., $\alpha > 0.5$). The

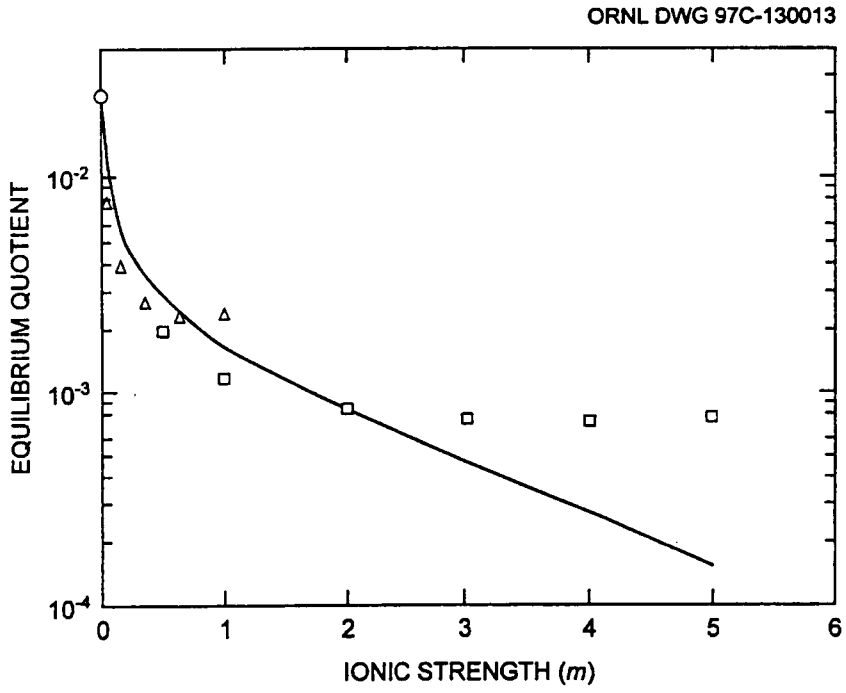

Figure 34. Equilibrium quotients for phosphate hydrolysis at 25°C. □ Ref. 46, △ Ref. 45, ○ Ref. 47, — this study.

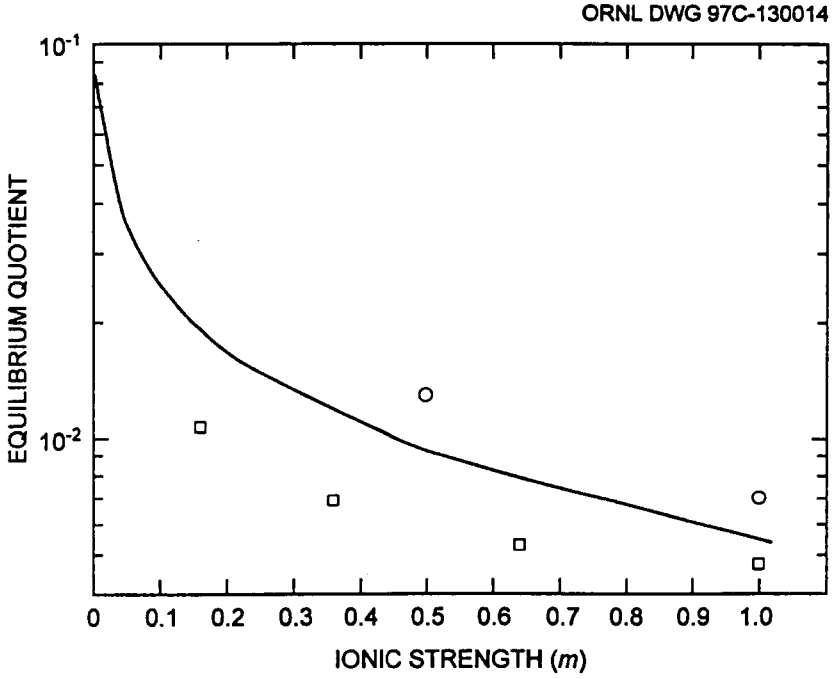

Figure 35. Equilibrium quotients for phosphate hydrolysis at 50°C. □ Ref. 45, ○ Ref. 48, — this study.

Table 10. Comparison of equilibrium quotients above 25°C

Temperature (°C)	Ionic strength (m)	Equilibrium quotient	
		Ref. 48	This study
50	0.5	-1.89	-2.04
	1.0	-2.15	-2.27
100	0.5	-1.14	-0.49
	1.0	-1.23	-0.76

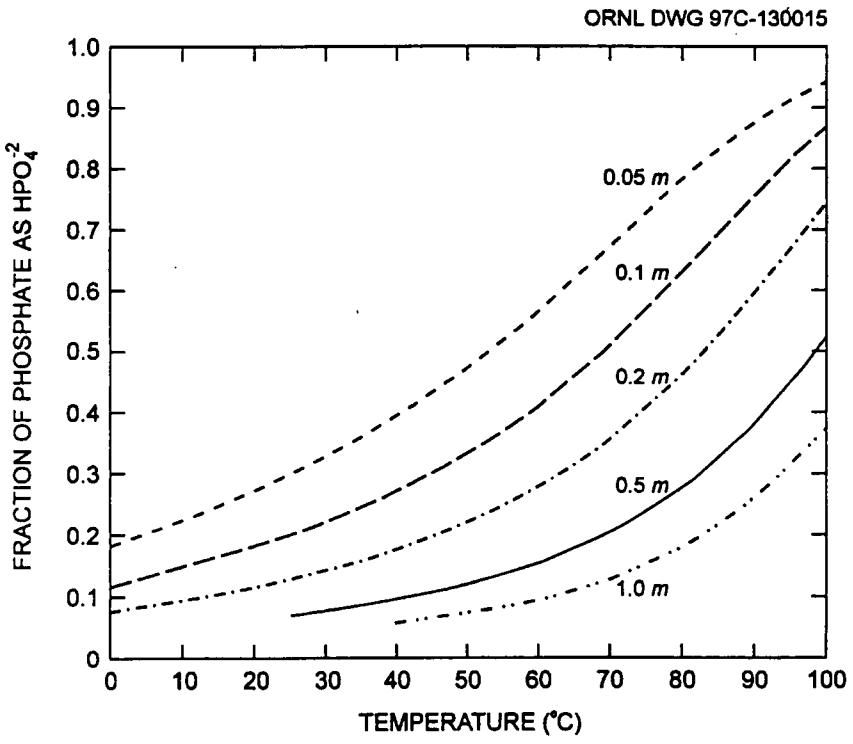

Figure 36. Association fraction for phosphate equilibria.

curves for 0.5 m and 1 m solutions do not extend to the lowest temperatures, since this would exceed the solubility limit.

5.2 Fluoride-Phosphate Experiments and Predictions

The solubility curve of sodium fluoride-phosphate solutions at 25 °C is shown in Fig. 37, for cases involving no excess OH^-, 1 m NaOH, and 3 m NaOH. For each hydroxide level, solubility of three different solids is depicted, with invariant points (where 2 solid phases are both present) appearing as corners on the curves. The hydroxide dependence is obvious, as solubility decreases drastically as OH^- increases, not only for the double salt, but for the simple salts TSP and NaF as well. It should be

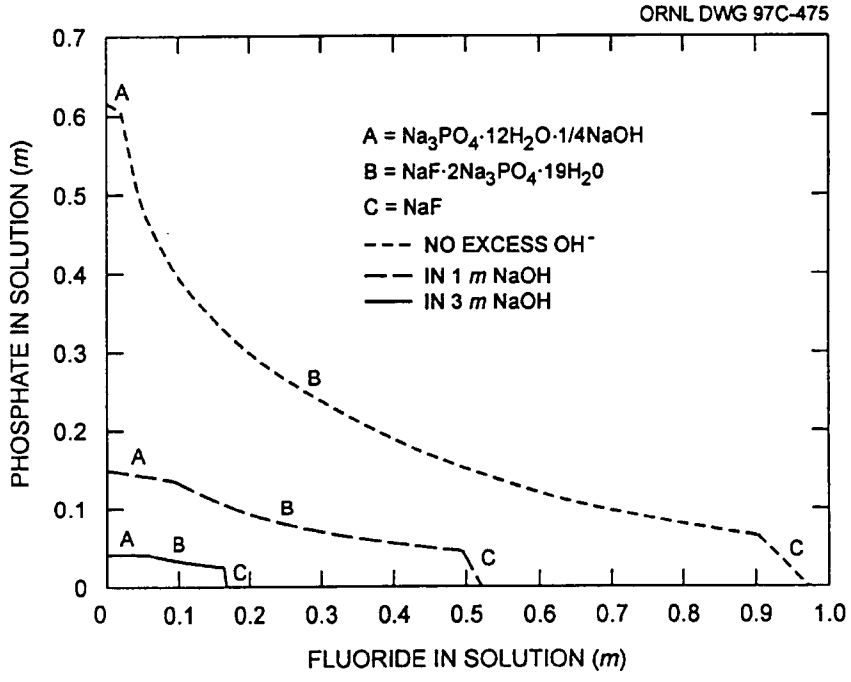

Figure 37. Prediction of solubilities in the Na-F-PO_4 system at 25 °C.

noted that the DS solubility in 3 m OH^- is an extrapolation, since no data were available. However, data were used for the simple salts in 3 m (and higher) OH^-, as well as the DS in 1 m OH^-. The predicted curve is fully consistent with these data.

In order to test these extrapolations, some qualitative experiments were run to ascertain general solubility behavior of solutions high in hydroxide (the region of primary interest for waste treatment). Stoichiometric amounts of H_3PO_4 and NaOH were mixed to obtain initial solutions containing exactly the mole ratio $Na/PO_4 = 3$. These were mixed with solutions containing NaF and NaOH in known amounts. Reagent grade chemicals and ultra-pure water, purified through ion-exchange membrane, were used throughout.

All components were mixed at about 60°C until total dissolution occurred. Subsequently, the solutions were cooled to 25°C and mixed for at least 1 day so they would come to equilibrium at the lower temperature. Precipitation (or lack thereof) was determined by visual examination, microscopic examination of crystals, and by X-ray diffraction. For a given starting concentration, these tests merely confirm whether or not precipitation of fluoride-phosphate species occurs. No attempt was made to measure aqueous concentrations of the mixed solution at equilibrium.

The individual data points in Fig. 38 denote initial concentrations of various experiments. Solid points indicate that solids formed (in every case, the precipitate was the DS), whereas, hollow data points indicate no precipitation. (For the point with $F^- = 0.1$ m, $PO_4^{-3} = 0.05$ m in 3 m OH^-, the analysis was indefinite.) In addition, the solubilities predicted by the model are reproduced here as continuous curves. These

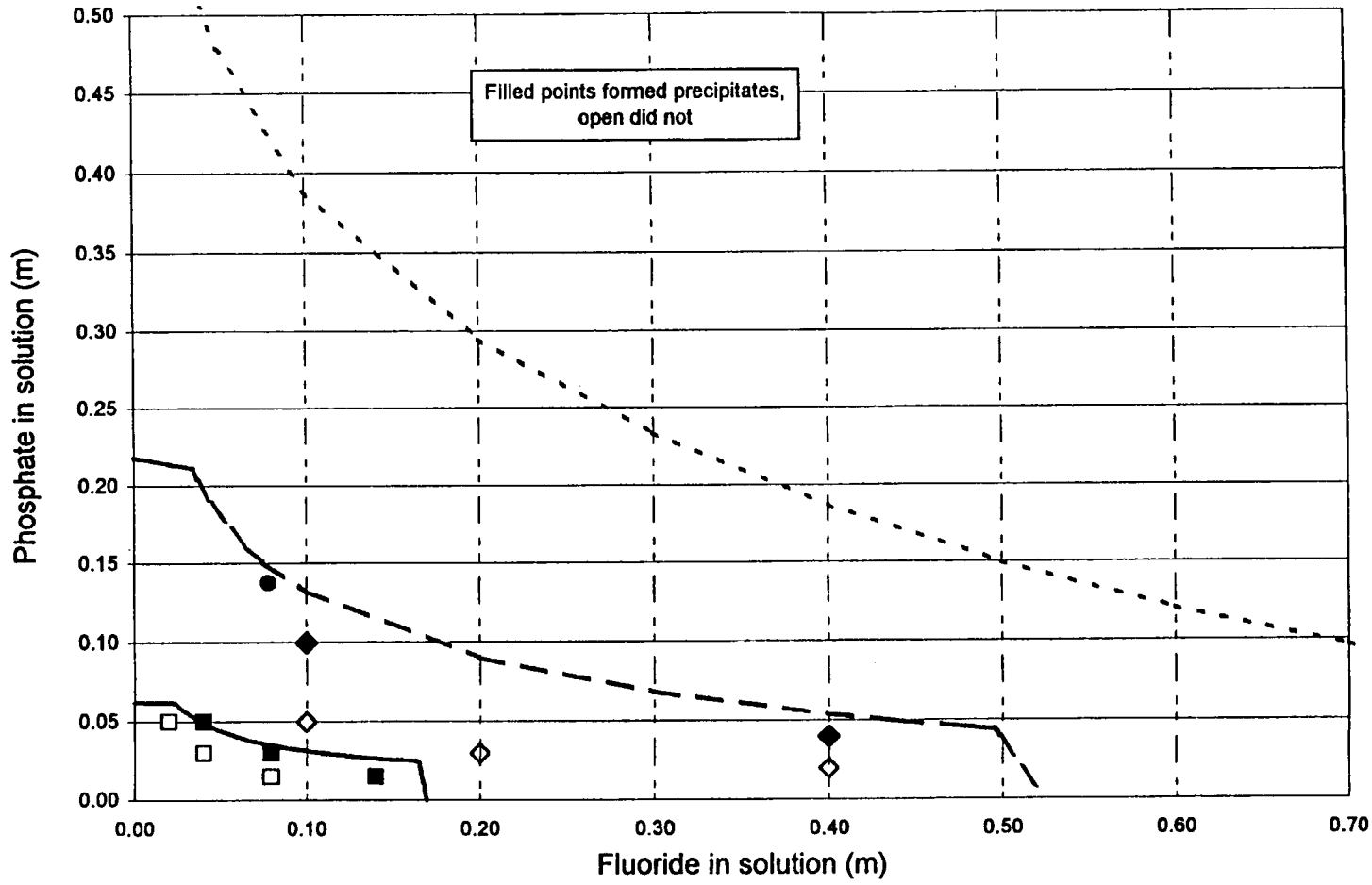

Figure 38. Qualitative data of double salt solubilities at 25°C. Model predictions: --- no added OH^-, – – – 1 m OH^-, —— 3 m OH^-. Data: ● Herting (1 M OH^-), ◇ ♦ in 1 m OH^-, □ ■ in 3 m OH^-.

curves differ slightly from those in Fig. 37, since the alternative chemical potential for TSP at 25°C was used (cf. p. 53). If the model prediction is accurate, then solid points should occur above the lines and open points below. As seen in the figure, the single point used in model formulation (in 1 M OH^- from Herting[28]) lies close to the predicted curve. The additional data indicate that the model generally overpredicts the ability of the DS to remain in solution. However, recall that these data are largely extrapolations. The predictions do match the qualitative behavior of the data through more than an order-of-magnitude change in solubility.

Finally, the temperature dependence of predictions was evaluated by mixing fluoride-phosphate solutions (in 3 m NaOH) at 100°C and cooling until solids formed. In order to minimize supersaturation effects, the solution temperature was lowered a short interval and held constant for many hours to permit equilibration. The three initial solutions shown in Table 11 all experienced onset of precipitation in the temperature interval 52-57°C. That is, no precipitation occurred in the equilibrium solution at 57°; but, solids did form as equilibrium was reached at 52°C. The model predictions are

Table 11. Prediction of precipitation temperature

Initial concentrations (m)			Temperature of precipitation (°C)	
F^-	PO_4^{-3}	OH^-	Data	Model
0.10	0.20	3	52-57	53
0.05	0.28	3	52-57	54
0.20	0.08	3	52-57	80 (NaF) 43 (DS)

shown in Table 11, and are consistent with observations in the first two cases. The third case is off, both in the prediction of NaF precipitation, and the prediction of DS forming at a lower temperature. As seen in Fig. 1, the prediction of NaF is highly uncertain, due to the large scatter in experimental data; hence, the model is not expected to be highly accurate in this regard. Considering that no fluoride-phosphate data were available at this high caustic concentration, the DS prediction is reasonable.

6. SUMMARY AND CONCLUSIONS

A thermodynamic model has been constructed which describes the phase-equilibrium behavior of solutions containing mixtures of NaF, Na_3PO_4, and NaOH over the temperature range 0-100°C. The model utilizes Pitzer's ion-interaction approach for electrolyte solutions, and a number of the necessary parameters have been determined in this study from data at various temperatures. Parameter estimation was accomplished by a nonlinear least-squares technique, applied to the whole system Na-F-PO_4-HPO_4-OH, and to the subsystems Na-F-OH, Na-HPO_4, and Na-PO_4-HPO_4-OH. Phase equilibria were determined by minimizing the total free energy, utilizing modifications to the code SOLGASMIX. The model itself was validated by comparison with many data points, including some qualitative solubility measurements done as part of this study.

The ion-interaction approach uses a number of input parameters in order to calculate activity coefficients in solutions of mixed electrolytes. A minimum requirement is a set of three coefficients for each binary system, i.e., for each cation-anion pair. Additional accuracy, especially for determination of phase equilibria, requires knowledge of ternary system coefficients — representing anion-anion pairs and triplets involving at least one anion and one cation. (Other systems might also require cation-cation parameters, but the present study did not, since Na^+ was the only cation of importance.)

In this study, each binary coefficient was determined by 3 parameters, representing the coefficient value at 25°C and two temperature coefficients. Values for

the pairs Na-F, Na-HPO_4, and Na-PO_4 were direct results of the analyses in this study. In addition, a number of ternary coefficients were also determined, although they were all assumed constant with respect to temperature.

In addition to activity coefficient parameters, determination of phase equilibria requires knowledge of free energies of formation. Values for most aqueous species (including water) were obtained from the literature. However, values for HPO_4^{-2} were obtained as a part of this study (valid through the temperature range 0-100°C. In addition, this study calculated free energies of formation for all solid species — NaF, TSP, DSP, and DS. Each of these quantities is temperature dependent over the range where solid formation occurs.

Model calculations were verified by reproducing the data used in parameter estimation. A variety of data were used, including isopiestic and e.m.f. measurements, freezing point lowering and vapor pressure lowering data, heat capacities, heats of dilution and solubilities. Phosphate hydrolysis was an intrinsic part of the model, and required special treatment in the utilization of enthalpy and heat capacity data.

The primary solid species are trisodium phosphate ($Na_3PO_4 \cdot 12\ H_2O \cdot ¼\ NaOH$), sodium fluoride (NaF), and the fluoride-phosphate double salt ($NaF \cdot 2\ Na_3PO_4 \cdot 19$ H2O). Predictions in regions of sparse data were less accurate, but reasonable. In general, the model tended to over-predict solubility of TSP in high caustic solutions at 25°C. This problem could be alleviated by modification of the free energy of formation for TSP, however, the result was no longer valid in regions of low caustic and high phosphate. Within the range 25-75°C, predictions of temperature effects on solubility of the DS were within the uncertainty of the data (about 10%). With regard to NaF, the large

scatter in solubility data creates more uncertainty in the model calculation. However, both are consistent in depicting only a slight increase in solubility with increasing temperature.

Qualitative solubility experiments were performed to evaluate overall model performance. These indicated that model predictions were good in regions where good data had been available in the parameter estimation process. Both the model predictions and experimental data have shown that solubility of each solid declines rapidly as hydroxide levels increase. In fact, for $OH^- \geq 3$ m, solubilities are so low that the error in measurement is of the same magnitude as the aqueous concentrations. For any hydroxide level, the presence of small amounts of either phosphate or fluoride will drastically reduce the solubility of the other. This effect is especially pronounced for small amounts of phosphate in predominantly fluoride solutions.

With regard to mixed waste treatment, this study shows that addition of caustic will reduce the solubility of both phosphate and fluoride, and that the solubility is lower still when both are present. Considerable increase in solubility can be achieved by raising the temperature above 65 °C. This is especially true of phosphate, since TSP does not form above this temperature and other phosphate species are much more soluble. It is also true of the DS, whose solubility rises steadily with temperature. It is not so true with NaF, whose solubility changes little with temperature. However, few wastes contain predominately fluoride, with little phosphate, and so this situation is not as relevant to waste processing operations.

If waste is processed in high caustic solutions at the higher temperature, great care must be taken to avoid supersaturation and uncontrolled precipitation. This

problem can be avoided by maintaining the high temperature, using a large excess of caustic (so that no precipitation occurs at ambient temperature), or implementing controlled precipitation with cooling. This last option not only avoids uncertainty and uncontrolled precipitation, but when combined with caustic recycle, may well have other practical advantages.

REFERENCES

REFERENCES

1. J. M. Simonson, R. E. Mesmer, and P. S. Z. Rogers, *J. Chem. Thermodynamics* **21**, 561 (1989).

2. K. S. Pitzer, "Ion Interaction Approach: Theory and Data Correlation," in K. S. Pitzer, ed., *Activity Coefficients in Electrolyte Solutions*, 2nd Ed., CRC Press, Boca Raton, Florida (1991).

3 W. F. Linke, *Solubilities*, 4th ed., Vol. II, D. Van Nostrand Co., Princeton, New Jersey (1958).

4. J.-C. Guiot, *Revue de Chemie minérale* **4**, 85 (1967).

5. R. A. Robinson, *J. Am. Chem. Soc.* **63**, 628 (1941).

6. R. W. Ivett and T. DeVries, *J. Am. Chem. Soc.* **63**, 2821 (1941).

7. W. J. Hamer and Y. C. Wu, *J. Phys. Chem. Ref. Data* 1(4), 1047 (1972).

8. *International Critical Tables*, Vol. IV, 258, McGraw-Hill, New York (1928).

9. *International Critical Tables*, Vol. III, 369, McGraw-Hill, New York (1928).

10. R. A. Robinson and R. H. Stokes, *Electrolyte Solutions*, 2nd ed., Butterworths, London, 1959.

11. J.-L. Fortier, P. A. Leduc, and J. E. Desnoyers, *J. Solution Chem.* **3**(4), 323 (1974).

12. H. W. Foote and J. F. Schairer, *J. Am. Chem. Soc.* **52**, 4202 (1930).

13. G. A. Lopatkina, *J. Appl. Chem of the USSR* **32** (12), 2722 (1959).

14. A. N. Campbell and A. J. R. Campbell, *Trans. Faraday Soc.* **35**, 241 (1939).

15. G. I. Nagorski and A. V. Nowosselos, *Zh. Obshch. Khim.* **5**, 182-4 (1935). See also Ref. 3, p. 1032.

16. S. L. Clegg and P. Brimblecombe, *J. Chem. Soc. Dalton Trans.*, 705 (1988).

17. R. F. Platford, *J. Chem. Eng. Data* **19**(2), 166 (1974).

18. G. Scatchard and R. C. Breckenridge, *J. Phys. Chem.* **58**, 596 (1954).

19. F. J. Millero, W. C. Duer, E. Shepard, and P. V. Chetirkin, *J. Solution Chem.* **7**(12), 877 (1978).

20. H. Bianchi and P. R. Tremaine, *J. Solution Chem.* **24**(5), 439 (1995).

21. J. W. Larson, K. G. Zeeb, and L. G. Hepler, *Can. J. Chem.* **60**, 2141 (1982).

22. *CRC Handbook of Chemistry and Physics*, 59th ed., p. D-305, CRC Press, Boca Raton, Florida (1978).

23. E. H. Loomis, *Phys. Rev.* **IV**(4), 273 (1897).

24. G. Tammann, *Wiedemann's Ann.* **24**, 523 (1885). For data tables, see J. Timmermans, *The Physico-chemical Constants of Binary Systems in Concentrated Solutions,* Vol. 3, p. 404, Interscience, New York (1960).

25. *Smithsonian Physical Tables*, 9th ed., p. 373, The Smithsonian Institution, Washington (1954).

26. B. Wendrow and K. A. Kobe, *Chem. Rev.* **54**, 891 (1954). see also B. Wendrow and K. A. Kobe, *Ind. Eng. Chem.* **44**(6), 1439 (1952).

27. C. W. Mason and E. B. Ashkroft, *Ind. Eng. Chem.* **31**(6), 768 (1939).

28. D. L. Herting, *Clean Salt Process Final Report*, Appendix A, WHC-EP-0915, Westinghouse Hanford Co. (1996).

29. O. N. Roslyakova, M. R. Petrov, and M. I. Zhikarev, *Russ. J. Inorg. Chem.* **24**(1), 115 (1979).

30. M. R. Petrov, O. N. Roslyakova, and M. I. Zhikharev, *Russ. J. Inorg. Chem.* **27**(6), 900 (1982).

31. T. M. Besmann, *SOLGASMIX-PV, a Computer Program to Calculate Equilibrium Relationships in Complex Chemical Systems*, ORNL/TM-5775, Union Carbide Corp., Nucl. Div., Oak Ridge Natl. Lab., 1977.

32. G. Eriksson, *Chemica Scripta* **8**, 100 (1975).

33. G. Eriksson and E. Rosén, *Chemica Scripta* **4**, 193 (1973).

34. G. Eriksson, *Acta. Chem. Scand.* **25**(7), 2651 (1971).

35. J. V. Beck and K. J. Arnold, *Parameter Estimation in Engineering and Science*, Wiley, New York (1977).

36. J. H. Seinfeld and L. Lapidus, *Mathematical Methods in Chemical Engineering*, Vol. 3, Prentice-Hall, Englewood Cliffs, New Jersey (1974).

37. R. Fletcher, *Practical Methods of Optimization*, Wiley, New York (1987).

38. D. Garvin, V. B. Parker, and H. J. White, *CODATA Thermodynamic Tables*, Hemisphere, Wash., 1987.

39. HSC Chemistry for Windows, Version 2.0, Outokumpu Research, May 31, 1994.

40. K. S. Pitzer, *J. Phys. Chem.* **77**, 268 (1973).

41. C. E. Harvie, N. Moller, and H. H. Weare, *Geochim. Cosmochim. Acta* **48**, 723 (1984).

42. K. S. Pitzer, *J. Amer. Chem. Soc.* **59**, 2365 (1937).

43. J. J. Christensen, R. M. Izatt, L. D. Hansen, and J. A. Partridge, *J. Phys. Chem.* **70**(6), 2003 (1966).

44. R. R. Irani and T. A. Taulli, *J. Inorg. Nucl. Chem.* **28**, 1011 (1966).

45. P. G. Daniele, A. De Robertis, C. De Stefano, A. Gianguzza, and S. Sammartano, *J. Solution Chem.* **20**(5), 495 (1991).

46. J. P. Hershey, M. Fernandez, and F. J. Millero, *J. Solution Chem.* **18**(9), 875 (1989).

47. C. E. Vanderzee and A. S. Quist, *J. Phys. Chem.* **65**, 118 (1961).

48. R. E. Mesmer and C. F. Baes, Jr., *J. Solution Chem.* **3**(4), 307 (1974).

APPENDICES

APPENDIX A

SUMMARY OF PARAMETERS IN CALCULATIONAL MODEL

APPENDIX A

SUMMARY OF PARAMETERS IN CALCULATIONAL MODEL

Table A.1. Free energies of formation $(\hat{\mu} = \mu^0/RT)$

Species	Temperature coefficients[a]				
	$\hat{\mu}_1$	$\hat{\mu}_2$	$\hat{\mu}_3 \times 10^{-7}$	$\hat{\mu}_4 \times 10^{-3}$	$\hat{\mu}_5 \times 10^{3}$
H_2O (l)	-95.665	-1.0029	0	0.32404	0.50848
Na^+ (aq)	-105.730	0.85194	0	0	-0.88327
H^+ (aq)	0	0	0	0	0
OH^- (aq)	-63.534	0.75606	0	0	-0.74688
Cl^- (aq)	-52.928	0.367999	0	0	0.35800
F^- (aq)	-112.590	1.13220	0	0	-1.14310
PO_4^{-3} (aq)	-411.192	4.33069	0	0	-4.36232
HPO_4^{-2} (aq)	-439.592	4.74018	0	0	-4.99770
NaCl (s)	-155.315	1.198614	0	0	-1.2000
NaF (s)	-219.391	2.022907	0	0	-2.08712
TSP[b] (s)	-1927.400	-1350.9963	-4.1882317	415.57092	731.17129
DSP[c] (s)	-1803.470	7.65392	0	0	0
DS[d] (s)	-3512.445	36.15256	0	0	-37.7395

[a]Coefficients for right hand side of Eq. (14).

[b]TSP = $Na_3PO_4 \cdot 12\ H_2O \cdot ¼\ NaOH$ (NOTE: All digits of accuracy are needed to accurately predict solubility behavior.).

[c]DSP = $Na_2HPO_4 \cdot 12\ H_2O$.

[d]DS = $NaF \cdot 2\ Na_3PO_4 \cdot 19\ H_2O$.

Table A.2. Activity coefficient parameters

		Temperature coefficient[b]		
Species[a]	Parameter	1	3	4
NaOH	$\beta^{(0)}$	0.0864	531.5	-1.625
NaOH	$\beta^{(1)}$	0.2530	894.4	-2.748
NaOH	C	0.0021	-40.69	0.116
Na-Cl	$\beta^{(0)}$	0.0759	280.3	-0.7339
Na-Cl	$\beta^{(1)}$	0.2765	-128.9	0.6430
Na-Cl	C	0.00065	-14.7	0.03392
Na-F	$\beta^{(0)}$	0.0330	246.8	-0.6728
Na-F	$\beta^{(1)}$	0.2456	2833.0	-9.451
Na-F	C	0.00281	12.25	-0.0436
Na-PO_4	$\beta^{(0)}$	0.2534	130.3	0.1247
Na-PO_4	$\beta^{(1)}$	3.7384	23420.0	-70.37
Na-PO_4	C	-0.02260	0	-0.00016
Na-HPO_4	$\beta^{(0)}$	-0.03045	1826.0	-5.159
Na-HPO_4	$\beta^{(1)}$	1.3504	6023.0	-18.77
Na-HPO_4	C	0.00359	-282.6	0.8267
OH-Cl	θ	-0.05		
OH-F	θ	0.1193		
Cl-F	θ	-0.01		
OH-PO_4	θ	0.1		
F-PO_4	θ	0.55		
Na-OH-Cl	ψ	-0.0063		
Na-OH-F	ψ	-0.035		
Na-OH-PO_4	ψ	0.03		
Na-Cl-F	ψ	-0.00218		

[a]All species are aqueous ions.

[b]Terms from Eq. (14); only coefficients 3 and 4 are used to describe temperature dependence.

APPENDIX B

UNSYMMETRICAL MIXING TERMS

FOR LIKE-CHARGED IONS

APPENDIX B

UNSYMMETRICAL MIXING TERMS FOR LIKE-CHARGED IONS

As mentioned in Section 3.3, when ions of like charge but different magnitude are present, the mixing term Φ_{ij} is dependent on ionic strength, as indicated in Eq. (13). A brief explanation and development of the theory is given in Ref. 2, where the dependency on ionic strength is given as

$$ {}^{E}\theta_{ij} = \frac{z_i z_j}{4I}\left[J(x_{ij}) - \frac{1}{2}J(x_{ii}) - \frac{1}{2}J(x_{jj})\right] \qquad \text{(B.1)} $$

where $x_{ij} = 6 z_i z_j A_\varphi \sqrt{I}$, and $J(x)$ is a complicated integral which must be solved numerically. Ref. 2 mentions a solution approach involving Chebychev polynomials, which was adopted and used throughout this work to determine both $J(x)$ and $J'(x) \equiv dJ/dx$. From the latter, and with use of Eq. (B.1), it is possible to calculate ${}^{E}\theta'_{ij} \equiv d\,{}^{E}\theta'_{ij}/dI$ from the equation[2]

$$ \hat{\theta}_{ij} \equiv {}^{E}\theta_{ij} + I\,{}^{E}\theta'_{ij} = \frac{z_i z_j}{8I}\left[x_{ij}J'(x_{ij}) - \frac{1}{2}x_{ii}J'(x_{ii}) - \frac{1}{2}x_{jj}J'(x_{jj})\right]. \qquad \text{(B.2)} $$

Various other derivatives of ${}^{E}\theta_{ij}$ arise in the use of the enthalpy and heat capacity data, which will now be considered.

From Eqs. (8) and (18), it is seen that $\partial {}^{E}\theta_{ij}/\partial T$ must be considered to adequately determine solution enthalpies. Such terms were ignored in Section 3.4, but will now be considered. First, note that

$$\frac{\partial x_{ij}}{\partial T} = 6z_i z_j \sqrt{I}\,\frac{\partial A_\varphi}{\partial T} = \frac{x_{ij}}{A_\varphi}\,\frac{dA_\varphi}{dT} = \frac{x_{ij}}{4RT^2}\cdot\frac{A_L}{A_\varphi} \tag{B.3a}$$

$$\frac{\partial x_{ij}}{\partial I} = 6z_i z_j A_\varphi \frac{1}{2\sqrt{I}} = \frac{x_{ij}}{2I}\,. \tag{B.3b}$$

Straightforward differentiation of Eq. (B.1) and substitution of Eqs. (B.2) and (B.3) then yields

$$\frac{\partial {}^{E}\theta_{ij}}{\partial T} = \frac{z_i z_j}{4T}\left[J'(x_{ij})\frac{\partial x_{ij}}{\partial T} - \frac{1}{2}J'(x_{ii})\frac{\partial x_{ii}}{\partial T} - \frac{1}{2}J'(x_{jj})\frac{\partial x_{jj}}{\partial T}\right] = \frac{A_L}{A_\varphi}\cdot\frac{\hat{\theta}_{ij}}{2RT^2}\,. \tag{B.4}$$

Calculation of the last term on the right is straightforward, and results in the following term to be added to the right hand side of Eq. (18):

$$+\frac{A_L}{A_\varphi}\frac{1}{2RT^2}\sum_{i=3}^{5}\sum_{j=i+1}^{6} m_i m_j \hat{\theta}_{ij}\,.$$

This term is clearly relevant in the case of phosphate solutions, where PO_4^{-3} is present with OH^- or HPO_4^{-2} or both.

When heat capacities of mixed solutions are used, it is also necessary to consider the additional derivatives $\partial^2 {}^{E}\theta/\partial T^2$, $\partial {}^{E}\theta'/\partial T$, and ${}^{E}\theta''$. Using Eqs. (B.1), (B.2), and (B.3), it can be shown that

$$I\frac{\partial\,{}^{E}\theta'_{ij}}{\partial T} = -\frac{1}{A_\varphi}\frac{\partial A_\varphi}{\partial T}(\hat{\theta}_{ij} + Q_{ij}) \tag{B.5}$$

$$2I\hat{\theta}'_{ij} = 2I\frac{\partial}{\partial I}({}^{E}\theta_{ij} + I\,{}^{E}\theta'_{ij}) = -\hat{\theta}_{ij} + Q_{ij} \tag{B.6}$$

where

$$Q_{ij} = \frac{z_i z_j}{8I}\left[x_{ij}^2 J''(x_{ij}) - \frac{1}{2}x_{ii}^2 J''(x_{ii}) - \frac{1}{2}x_{jj}^2 J''(x_{jj})\right]. \tag{B.7}$$

Numerical calculations through the temperature range 0-100°C indicate that Q_{ij} contributes less than 1% to the right hand sides of Eqs. (B.5) and (B.6) for $I \geq 0.2$. In such cases, the approximation $Q_{ij} = 0$ introduces negligible error. As I decreases below 0.2, the contribution of Q_{ij} steadily increases, becoming quite significant for $I < 0.01$. However, the importance of the mixture parameters generally for $I < 0.2$ is negligible. Hence, we can assume $Q_{ij} = 0$ will result in excellent approximations of Eqs. (B.5)-(B.6).

Including the mixture terms of Eq. (8) will result in the following additions to equations in Appendix C:

1. Appended to Eq. (C.5):

$$\ldots + \frac{A_L}{A_\varphi}\frac{m^2}{2RT^2}\left\{\left[(1-\alpha) + \alpha\xi_2\right](\hat{\theta}_{34} + \hat{\theta}_{35}) + \alpha(\eta_2 + 1)\hat{\theta}_{45} + \frac{\alpha}{2I}\frac{dI}{d\alpha}\left[(1-\alpha)(\hat{\theta}_{34} + \hat{\theta}_{35}) + \alpha\hat{\theta}_{45}\right]\right\}.$$

2. Appended to Eq. (C.7):

$$\ldots + \frac{\alpha m^2 A_L}{2RT^2 A_\varphi}\left[(1-\alpha)\left(\hat{\theta}_{34}+\hat{\theta}_{35}\right) + \alpha\,\hat{\theta}_{45}\right].$$

3. Appended to Eq. (C.8):

$$\ldots + 2m^2\left\{\left[(1-\alpha)+\alpha\xi_2\right]\left[\Phi^{\varphi}_{34}+\Phi^{\varphi}_{35} + 3m\left(\psi_{234}+\psi_{235}\right)\right] + \alpha\left(\eta_2+1\right)\left(\Phi^{\varphi}_{45}+3m\,\psi_{245}\right)\right.$$

$$\left. + \frac{\alpha}{2I}\frac{\mathrm{d}I}{\mathrm{d}\alpha}\left[(1-\alpha)\left(\hat{\theta}_{34}+\hat{\theta}_{35}\right)+\alpha\,\hat{\theta}_{45}\right] + \frac{3m^2}{\Omega}\left[(1-\alpha)\left(\psi_{234}+\psi_{235}\right)+\alpha\,\psi_{245}\right]\right\}.$$

4. Appended to Eq. (C.9):

$$\ldots + \frac{A_L}{A_\varphi}\cdot\frac{m}{2RT^2}\left[(2\alpha-1)(\hat{\theta}_{34}+\hat{\theta}_{35}) - 2\alpha\,\hat{\theta}_{45}\right].$$

5. Appended to Eq. (C.10):

$$\ldots + 2m(\eta_1-\xi_1)(\Phi_{34}+\Phi_{35}) + 2m(2\alpha-1)({}^{E}\theta'_{34}+{}^{E}\theta'_{35}) + 3m^2(\eta_2-\xi_2)(\psi_{234}+\psi_{235})$$

$$-4m(\eta_1\Phi_{45}+\alpha\,{}^{E}\theta'_{45}) - 6m^2\eta_2\psi_{245}\,.$$

APPENDIX C

USE OF TOTAL SOLUTION HEAT CAPACITIES WHEN CHEMICAL REACTION OCCURS

APPENDIX C

USE OF TOTAL SOLUTION HEAT CAPACITIES WHEN CHEMICAL REACTION OCCURS

As shown in Sect. 3.4 for enthalpy data, heat capacity data also contain effects due to both the hydrolysis reaction and solvation. Recognizing that the process of solvation from crystalline solid is not involved in heat capacity measurements, Eq. (15) can be rewritten

$$L_{\varphi,TOT} = \alpha\ \Delta H_r^0 + L_\varphi\ , \tag{C.1}$$

where ΔH_r^0 and L_φ are given by Eqs. (17) and (19), respectively. Then the apparent molar heat capacity of the total solution is obtained from the total temperature derivative of Eq. (C.1):

$$C_p - C_p^0 = \frac{dL_{\varphi,TOT}}{dT} = \alpha\left(\frac{\partial \Delta H_r^0}{\partial T}\right)_{m_t} + \left(\frac{\partial L_\varphi}{\partial T}\right)_{m_t} + \left[\Delta H_r^0 + \left(\frac{\partial L_\varphi}{\partial \alpha}\right)_T\right]\frac{\partial \alpha}{\partial T}\ . \tag{C.2}$$

Differentiating Eq. (17), it can easily be determined that

$$\frac{\partial \Delta H_r^0}{\partial T} = -R\left(2\Delta\hat{\mu}_2 T + \Delta\hat{\mu}_4 + 6\Delta\hat{\mu}_5 T^2\right)\ . \tag{C.3}$$

Also, recognizing that $\partial L_\varphi/\partial T$ affects only the explicit dependence on T of the terms A_L, $B_{ij}^{\,L}$, and $C_{ij}^{\,L}$, differentiation and rearrangement of Eq. (19) produces

$$\left(\frac{\partial L_\varphi}{\partial T}\right)_m = \frac{2(3-\alpha)}{b} A_J \ln\left(1+b\sqrt{I}\right) - 6RT^2 m\left[(1-\alpha)\left(B_{23}^{\,J}+3mC_{23}^{\,J}\right)+\alpha\left(B_{24}^{\,J}+B_{25}^{\,J}+3m\left(C_{24}^{\,J}+C_{25}^{\,J}\right)\right)\right], \qquad \text{(C.4)}$$

where $A_J = \dfrac{\partial A_\varphi}{\partial T}$, $\quad B_{ij}^{\,J} = \dfrac{2}{T}B_{ij}^{\,L} + \dfrac{\partial B_{ij}^{\,L}}{\partial T}$, $\quad C_{ij}^{\,J} = \dfrac{2}{T}C_{ij}^{\,L} + \dfrac{\partial C_{ij}^{\,L}}{\partial T}$.

The next step is to determine derivatives involving α. First, note that

$$\frac{dm}{d\alpha} = \frac{d}{d\alpha}\left(\frac{N_2\Omega}{N_1-\alpha N_2}\right) = \frac{m^2}{\Omega},$$

$$\frac{dI}{d\alpha} = -2m + 2(3-\alpha)\frac{dm}{d\alpha} = 2m\left[\frac{I}{2\Omega}-1\right].$$

Then Eq. (19) is differentiated with respect to α; after some rearranging, this results in

$$\frac{\partial L_\varphi}{\partial \alpha} = A_L\left[-\frac{2}{b}\ln\left(1+b\sqrt{I}\right)+\frac{\sqrt{I}}{I+b\sqrt{I}}\left(\frac{I}{2\Omega}-1\right)\right] - 6mRT^2\left\{\xi_1 B_{23}^{\,L}+\eta_1\left(B_{24}^{\,L}+B_{25}^{\,L}\right)+3m\left[\xi_2 C_{23}^{\,L}+\eta_2\left(C_{24}^{\,L}+C_{25}^{\,L}\right)\right] + \frac{dI}{d\alpha}\left[(1-\alpha)B_{23}^{\,L\prime}+\alpha\left(B_{24}^{\,L\prime}+B_{25}^{\,L\prime}\right)\right]\right\}. \qquad \text{(C.5)}$$

where $\xi_j \equiv (1-\alpha)\dfrac{jm}{\Omega}-1$, $\quad \eta_j \equiv \dfrac{j\alpha m}{\Omega}+1$,

and

$$B^{L\prime} = \frac{\partial B^{L}}{\partial I} = \frac{\partial B'}{\partial T} = \frac{\partial \beta^{(1)}}{\partial T} \cdot \frac{1}{I} g'\left(\alpha\sqrt{I}\right), \quad g'(x) = -\frac{2}{x^2}\left[1 - (1 + x + \frac{x^2}{2})e^{-x}\right].$$

Finally, to determine the quantity $\partial\alpha/\partial T$, it is necessary to consider again the hydrolysis reaction (4). The equilibrium free energy change is

$$\Delta\hat{\mu}_r = \left(\hat{\mu}_4 + \hat{\mu}_5 - \hat{\mu}_1 - \hat{\mu}_3\right) = -\ln\frac{a_4 a_5}{a_1 a_3} = -\frac{\varphi m}{\Omega}(4+\alpha) + \ln\frac{(1-\alpha)}{\alpha^2} - \ln m + \ln\Gamma$$

where $\Gamma \equiv \gamma_3/\gamma_4\gamma_5$. As was done for Eq. (17), this is differentiated with respect to T,

$$-\frac{\Delta H_r^0}{RT^2} = \frac{\partial}{\partial T}\left(\Delta\hat{\mu}_r\right)_{m_i}$$
$$= -\frac{1}{\Omega}\frac{\partial}{\partial T}\left[\varphi m(4+\alpha)\right] + \frac{\partial \ln\Gamma}{\partial T} - \frac{\partial\alpha}{\partial T}\left[\frac{1}{\Omega}\frac{\partial}{\partial\alpha}\left[\varphi m(4+\alpha)\right] - \frac{\partial}{\partial\alpha}(\ln\Gamma) + \frac{2-\alpha}{\alpha(1-\alpha)} + \frac{m}{\Omega}\right],$$

which can be rearranged to yield the final form

$$\frac{\partial\alpha}{\partial T} = \frac{\dfrac{\partial \ln\Gamma}{\partial T} - \dfrac{1}{\Omega}\dfrac{\partial}{\partial T}\left[\varphi m\,(4+\alpha)\right] + \dfrac{\Delta H_r^0}{RT^2}}{\dfrac{1}{\Omega}\dfrac{\partial}{\partial\alpha}\left[\varphi m(4+\alpha)\right] + \dfrac{m}{\Omega} + \dfrac{2-\alpha}{\alpha(1-\alpha)} - \dfrac{\partial \ln\Gamma}{\partial\alpha}}. \qquad \text{(C.6)}$$

The various terms in Eq. (C.6) are determined as follows. Substituting $Z = 6\,m$ into Eq. (10) and rearranging yields:

$$P \equiv m(4+\alpha)\varphi$$
$$= m(4+\alpha) - \frac{2A_\varphi I^{3/2}}{1+b\sqrt{I}} + 6m^2\left[(1-\alpha)\left(B_{23}^{\varphi} + 6mC_{23}\right) + \alpha\left(B_{24}^{\varphi} + 6mC_{24}\right) + \alpha\left(B_{25}^{\varphi} + 6mC_{25}\right)\right].$$

Differentiation with respect to T (at constant α) gives

$$\frac{\partial P}{\partial T} = -\frac{A_L}{2RT^2}\frac{I^{3/2}}{1+b\sqrt{I}}$$
$$+ 6m^2\left[(1-\alpha)\left(B_{23}^{\varphi L} + 6mC_{23}^{L}\right) + \alpha\left(B_{24}^{\varphi L} + 6mC_{24}^{L}\right) + \alpha\left(B_{25}^{\varphi L} + 6mC_{25}^{L}\right)\right] \qquad \text{(C.7)}$$

where $B_{ij}^{\varphi L} = \frac{\partial B_{ij}^{\varphi}}{\partial T} = \frac{\partial \beta_{ij}^{(0)}}{\partial T} + \frac{\partial \beta_{ij}^{(1)}}{\partial T}\exp\left(-\alpha\sqrt{I}\right).$

Differentiation with respect to α (at constant T) gives:

$$\frac{\partial P}{\partial \alpha} = \frac{m^2}{\Omega}(4+\alpha) + m - A_\varphi\frac{\sqrt{I}\left(3+2b\sqrt{I}\right)}{\left(1+b\sqrt{I}\right)^2}\frac{dI}{d\alpha} + 6m^2\left\{\xi_2 B_{23}^{\varphi} + \eta_2\left(B_{24}^{\varphi} + B_{25}^{\varphi}\right)\right.$$
$$\left. + 6m\left[\xi_3 C_{23} + \eta_3\left(C_{24} + C_{25}\right)\right] + (1-\alpha)\frac{\partial B_{23}^{\varphi}}{\partial \alpha} + \alpha\left(\frac{\partial B_{24}^{\varphi}}{\partial \alpha} + \frac{\partial B_{25}^{\varphi}}{\partial \alpha}\right)\right\}, \qquad \text{(C.8)}$$

where $\frac{\partial B_{ij}^{\varphi}}{\partial \alpha} = \frac{\partial B_{ij}^{\varphi}}{\partial I}\frac{dI}{d\alpha} = \frac{dI}{d\alpha}\frac{\partial}{\partial I}\left[\beta^{(0)} + \beta^{(1)}\exp\left(-\alpha\sqrt{I}\right)\right] = \frac{dI}{d\alpha}\beta^{(1)}\frac{\alpha}{2\sqrt{I}}\exp\left(-\alpha\sqrt{I}\right).$

Now, realizing that $z_3 = -3$, $z_4 = -2$, and $z_5 = -1$, Eq. (11b) can be used to obtain

$$\ln\Gamma = -4A_\varphi\left[\frac{\sqrt{I}}{1+b\sqrt{I}} + \frac{2}{b}\ln\left(1+b\sqrt{I}\right)\right] + 12m^2\left[(1-\alpha)B_{23}' + \alpha\left(B_{24}' + B_{25}'\right)\right]$$
$$+ 6m\left[\left(B_{23} - B_{24} - B_{25}\right) + 3m\left(C_{23} - C_{24} - C_{25}\right)\right].$$

Differentiating with respect to temperature (at constant α) gives:

$$\frac{\partial \ln \Gamma}{\partial T} = -\frac{A_L}{RT^2}\left[\frac{\sqrt{I}}{1+b\sqrt{I}} + \frac{2}{b}\ln\left(1+b\sqrt{I}\right)\right] + 12m^2\left[(1-\alpha)B_{23}^{L\prime} + \alpha\left(B_{24}^{L\prime} + B_{25}^{L\prime}\right)\right]$$

$$+ 6m\left[\left(B_{23}^{L} - B_{24}^{L} - B_{25}^{L}\right) + 3m\left(C_{23}^{L} - C_{24}^{L} - C_{25}^{L}\right)\right]. \qquad \text{(C.9)}$$

Finally, differentiating with respect to α (at constant T) yields:

$$\frac{\partial \ln \Gamma}{\partial \alpha} = -2A_{\varphi}\frac{dI}{d\alpha}\frac{(3+2b\sqrt{I})}{\sqrt{I}(1+b\sqrt{I})^2} + 12m^2[\xi_2 B_{23}' + \eta_2(B_{24}' + B_{25}')]$$

$$+ 12m^2\frac{dI}{d\alpha}[(1-\alpha)B_{23}'' + (B_{24}'' + B_{25}'')] + 6m\frac{dI}{d\alpha}l(B_{23}' - B_{24}' - B_{25}')$$

$$+ 6\frac{m^2}{\Omega}[(B_{23} - B_{24} - B_{25}) + 6m(C_{23} - C_{24} - C_{25})]\,. \qquad \text{(C.10)}$$

Since, $B' = \beta^{(1)} g'(x)/I$, then it can be determined that

$$B'' = \frac{\partial B'}{\partial I} = \frac{\beta^{(1)}}{I^2}\cdot\frac{4}{x^2}\left[1 - \left(1 + x + \frac{x^2}{2} + \frac{x^3}{8}\right)e^{-x}\right].$$

Substitution of Eqs. (C.7) - (C.10) into Eq. (C.6) allows calculation of $d\alpha/dT$. The heat capacity can then be calculated from Eq. (C.2), using Eqs. (C.3)-(C.6) and Eq. (17), with C_p^0 treated as an adjustable parameter.

The complexity in calculating various terms of Eqs. (C.2) and (C.6) causes us to consider simplifying these expressions. However, it is not known *a priori* which terms to keep and which to omit. It is thus instructive to consider the relative magnitudes for various terms at the molalities of the principal data used, from Ref. 20. This is done in Tables C.1 and C.2, using the optimal parameters from Section 4.

Table C.1. Relative values of terms in Eq. (C.2)

m	C_p^0	$\Delta H_r^0 \frac{\partial \alpha}{\partial T}$	$\frac{\partial L_\varphi}{\partial \alpha} \frac{\partial \alpha}{\partial T}$	$\alpha \frac{\partial \Delta H_r^0}{\partial T}$	$\frac{\partial L_\varphi}{\partial T}$	C_p^{rel}	C_p^{spec}
0.05492	-507.7	182.5	-1.7	93.3	157.7	180.8	-256.7
0.09009	-507.7	143.9	-1.2	69.6	211.5	142.6	-226.6
0.11229	-507.7	127.8	-1.2	60.8	238.1	126.5	-208.8
0.22570	-507.7	83.7	-1.9	38.7	329.3	81.8	-139.7
0.32853	-507.7	65.0	-2.5	30.1	378.6	62.5	-99.1
0.46314	-507.7	50.9	-2.8	23.7	420.9	48.0	-63.1

Table C.2. Relative values of terms in Eq. (C.6)

m	$\frac{\Delta H_r^0}{RT^2}$	$\frac{\partial P/\Omega}{\partial T} \times 10^6$	$\frac{\partial \ln \Gamma}{\partial T} \times 10^4$	$\frac{m}{\Omega} \times 10^3$	$\frac{2-\alpha}{\alpha(1-\alpha)}$	$\frac{\partial P/\Omega}{\partial \alpha} \times 10^3$	$\frac{\partial \ln \Gamma}{\partial \alpha} \times 10^2$
0.05492	0.0458	0.7	-4.4	1.0	8.4	1.4	0.3
0.09009	0.0458	2.1	-4.0	1.6	10.7	2.3	-0.6
0.11229	0.0458	3.2	-4.5	2.0	12.0	2.9	-1.1
0.22570	0.0458	9.9	-10.6	4.1	18.1	6.1	-3.5
0.32853	0.0458	17.5	-17.5	5.9	22.9	9.1	-5.6
0.46314	0.0458	30.3	-25.4	8.4	28.7	1.3	-8.0

In Table C.1, it is seen that all terms except the one involving $\partial L_\varphi/\partial\alpha$ are significant in Eq. (C.2), and must be included. In the last two columns are the terms C_p^{rel} and C_p^{spec} as defined in Ref. 20. The former (termed the "relaxation" component) consists of all contributions to C_p which depend on the chemical reaction or $d\alpha/dT$. Hence, $C_p^{rel} = 0$ if no reaction takes place (i.e., α is constant). The other term (the "species" component) is the sum of the remaining terms in Eq. (C.2). The values shown in Table C.1 for these two quantities agree fairly well with those in Ref. 26, which were obtained from an approximation to Eq. (C.2), and used only C_p data.

From Table C.2, we see that numerator and denominator of Eq. (C.6) are each dominated by a single term. To a good approximation, then

$$\frac{d\alpha}{dT} \cong \frac{(2-\alpha)\,\Delta H_r^0}{\alpha(1-\alpha)\,RT^2}\,.$$

APPENDIX D

LIST OF SYMBOLS

APPENDIX D

LIST OF SYMBOLS

Roman Characters

a_i	activity of species i
A_φ	Debye-Hückel coefficient [Eq. (9b)]
A_L	Temperature derivative of Debye-Hückel coefficient [Eq. (18)]
A_J	Second temperature derivative of Debye-Hückel coefficient [Eq. (C.4)]
b	fixed constant in Debye-Hückel term [Eq. (9b)]
B_{ij}, B_{ij}^{φ}	ion-interaction parameters [Eq. (8)]
B_{ij}^{L}, $B_{ij}^{L\varphi}$	Temperature derivative of B_{ij}, B_{ij}^{φ} [Eqs. (18), (C.7)]
B_{ij}^{J}	Second temperature derivative of B_{ij} [Eq. (C.4)]
C_{ij}	ion-interaction parameters [Eq. (8)]
C_{ij}^{L}	Temperature derivative of C_{ij} [Eq. (18)]
C_{ij}^{J}	Second temperature derivative of C_{ij} [Eq. (C.4)]
$\mathbf{e}$	vector of error residuals [Eq. (6)]
E	total sum of squared error [Eq. (6)]
C_p	heat capacity
C_p^0	heat capacity at infinite dilution
f	Debye-Hückel term [Eqs. (8), (9)]
F	expanded Debye-Hückel term [Eq. (12d)]
g	activity coefficient function [Eq. (9a)]
G	total Free Energy [Eq. (5)]
$\bar{G}_i$	partial molar free energy of species i [Eq. (5)]

G_i^0	molar free energy of formation for species *i*
G^{ex}	excess free energy for total solution [Eq. (8)]
H	solution enthalpy
H^0	solution enthalpy at infinite dilution
ΔH_{dil}	enthalpy change of dilution
ΔH_s	enthalpy change of solvation
ΔH_r	enthalpy change of reaction
i	species index
I	ionic strength [Eq. (9)]
j	species index
$J(x)$	integral in Appendix B
L	relative solution enthalpy
L_φ	apparent relative solution enthalpy [Eq. (15)]
m	molality (mol/kg), stoichiometric molality [Eq. (19)]
m_i	molality of species *i*
M	molarity (mol/L)
M_1	mass of water (kg)
n_i	mole inventory of species *i*
N_i	initial mole inventory of species *i*
$\mathbf{p}$	vector of parameters to be optimized [Eq. (6)]
P	multiple of osmotic coefficient [Eq. (C.7)]
R	gas constant
T	temperature (°C or K)
T_0	standard temperature (25°C) [Eq. (14)]
$\mathbf{V}$	data covariance matrix [Eq. (6)]
x	mole fraction (p. 9), general variable [Eq. (9a)]
x_i, $\hat{x}_i$	components of calculated and data vectors [Eq. (6)]

x_{ij}	argument in Eq. (B.1)
$\mathbf{x}$	vector of calculated quantities [Eq. (6)]
$\hat{\mathbf{x}}$	vector of data points [Eq. (6)]
z_i	charge on ion i
Z	absolute charge sum [Eq. (12a)]

Greek Characters

α	constant in Pitzer equations [Eq. (9a)], association fraction [Eq. (19)]
$\beta_{ij}^{(0)}$, $\beta_{ij}^{(1)}$	ion-interaction parameters [Eq. (8)]
γ	general activity coefficient
γ_i	activity coefficient of species i
Γ	activity coefficient ratio [Eq. (C.6)]
η_j	coefficient [Eq. (C.5)]
θ_{ij}, ${}^{E}\theta_{ij}$	components of Φ_{ij} [Eq. (13)]
μ_i^0	standard chemical potential of species i
$\hat{\mu}_i$	reduced standard chemical potential of species i [Eq. (14)]
$\hat{\mu}_{ij}$	temperature coefficients in $\hat{\mu}_i$ representation [Eq. (14)]
$\Delta\hat{\mu}_r$	reduced free energy change for reaction
$\Delta\hat{\mu}_j$	temperature coefficients of $\Delta\mu_r$
ν	sum of stoichiometric coefficients in dissolved solid [Eq. (20)]
ν_i	stoichiometric coefficient of ion i in dissolved solid [Eq. (20)]
ξ_j	coefficient [Eq. (C.5)]
σ	vector of standard errors in data
σ_j	standard error (std. deviation) for data point j
φ	osmotic coefficient
Φ_{ij}, Φ_{ij}^{φ}	ion-interaction parameters [Eq. (8)]
ψ_{ijk}	ion-interaction parameter [Eq. (8)]

Ω	solvent moles per kilogram ($\Omega = 55.51$ for water)

Acronyms

e.m.f.	electro-motive force
TSP	trisodium phosphate: $Na_3PO_4 \cdot 12\ H_2O \cdot ¼\ NaOH$
DSP	disodium phosphate: $Na_2HPO_4 \cdot 12\ H_2O$
DS	double salt: $NaF \cdot 2\ Na_3PO_4 \cdot 19\ H_2O$

VITA

Charles F. Weber was born in Tucson, Arizona on August 13, 1953. He graduated in 1971 from Oak Ridge High School in Oak Ridge, Tennessee. He then attended The University of Tennessee-Knoxville, where in 1975 he received a Bachelor of Arts Degree, majoring in mathematics and minoring in computer science. Continuing his studies there, he received three Master of Science degrees, in management science (1976), mathematics (1979), and chemical engineering (1990). In September 1976, Mr. Weber accepted a teaching assistantship in the Mathematics Department of The University of Tennessee. In January 1978, he began a research assistantship with the Nuclear Engineering Department, in conjunction with the Oak Ridge National Laboratory (ORNL). He later was employed by ORNL, joining the Computer Sciences Division in October 1978. At ORNL, his research has touched several areas of applied mathematics, chemistry, and chemical engineering. Most recently, he has been involved in optimization theory and aqueous electrolyte thermodynamics.

In addition to two previous theses, Mr. Weber has authored or contributed to a number of reports and open literature publications. He is a member of the American Institute of Chemical Engineers and the Society for Industrial and Applied Mathematics.

Mr. Weber is married to the former Renee Rios and is the father of five daughters, Cristina, Alicia, Lilia, Marcela, and Sara Emma.